Investigation on High Performance Coating by Plasma Processing

May 2018

NAGASAKI UNIVERSITY

GRADUATE SCHOOL OF ENGINEERING

Musab Timan Idriss Gasab

Contents

Chapter 3

Influence of physical conditions on extended anode effect in tube inner coating

Chapter 4

Tube inner coating of non-conductive films by pulsed reactive coaxial magnetron plasma with outer anode

Chapter 5

Conclusions

Chapter 1

Introduction

This thesis reports investigations on high performance coating by plasma processing. Coating with functional materials is attracting attention in various fields including industrial and medical fields, because it can desirably change surface properties of materials. Plasma processing is widely used in coating, because a very wide variety of thin films such as pure metals, alloys, etc. can be deposited. However, it is very challenging to conduct inner coatings of narrow tubes. It is also challenging to conduct coatings of non-conductive materials on non-conductive substrates. In this study, the author aimed to develop new methods to realize these difficult but necessary coatings in high performance. Consequently, the author has developed methods to conduct coating of non-conductive films on inner and outer walls of non-conductive tubes. The coated thin films were in acceptable performance. This chapter describes background, scope, purpose, etc. in detail.

1.1 Coating

Coating is the process of covering the surface of materials by decorative or functional film according to the desired properties. The process might be complete or partial coating of the substrate. The advantage of coating is that the substrate material will be able to gain new properties according to the properties of the coated film. Coating process is widely used in industry for many purposes. There are many coating methods which are from hand brush to plasma technology, depending on the

characteristics of the desired film. Today, plasma coating has become the major coating technology.

Coating is utilized in many fields of industries. However, it is difficult to make coating on inner walls of narrow tubes. They will be used in the field of gas or liquid transportation. In these fields, new technology is required. In the fields of medicine, new coating technology for cylindrical substrate such as catheter is desired. For catheter adding biocompatibility and low friction coefficient are required.

1.2 Introduction to Plasma

Despite the conventional belief that our universe consists of the three states of matter (solid, liquid and gas), there is another state which is plasma. It is called the fourth state of matter. More specifically, plasma is an ionized gas or other medium in which charged particle interactions are predominant. Here "ionized gas" means a collective of particles in which there are considerable numbers of "free (unbound) electrons" and "electrically charged ions" in addition to the neutral atoms and molecules, which are normally present in a gas. Therefore, the charged particles interact with many other particles in the plasma. Therefore, the charged particles interact with many other particles in the plasma. The plasma is a collective but weakly coupled medium in which interaction energies are much smaller than thermal energies [A1]. The atoms or molecules convert into positively charged ions during ionization. In addition, the condition of "Debye's sphere" has to be accomplished, which determines the quasi-neutral state [A2].

Most likely, we live in 1% of the universe in which plasmas is not generated naturally, while the 99% of the matter in the universe is in plasma state [A3]. This

assessment may not be precise but it is undoubtedly rational, because stellar interiors and atmospheres, gaseous nebulae, and most of the interstellar hydrogen are plasmas. In our own neighborhood, one encounters the plasma comprising the Van Allen radiation belts and the solar wind soon after one leaves from the earth's atmosphere. On the other hand, in our daily lives, there are encounters with plasma such as Aurora Borealis, fluorescent light, neon sign, and lightning [A3].

Plasma technology can be divided into thermal and non-thermal plasma from aspect of gas temperature. On the other hand, from the aspect of material phase, plasma technology can be divided into solid phase, gas phase and liquid phase plasma technologies. Gas-phase plasma technology is widely used in many industrial fields, such as electronic device manufacturing processes (e.g. plasma etching, sputtering, plasma-enhanced chemical vapor deposition, etc.), hard coating processes (e.g. ion plating, sputtering, etc.), and surface treatment processes (low or atmospheric pressure plasma treatments, sputtering, plasma etching, etc.). Solid-phase plasma technology has been used in surface-Plasmon resonance (SPR) spectroscopy, etc. It is also used for healthcare, analysis, paint, etc. [A4]. Liquid-phase plasma technology also has large application fields (e.g. nano-material synthesis, surface modification, water treatment, sterilization, recycle of rare materials, and decomposition of toxic compounds) [A5]. Plasma processing dealt in this study is related to the gas phase plasma technology.

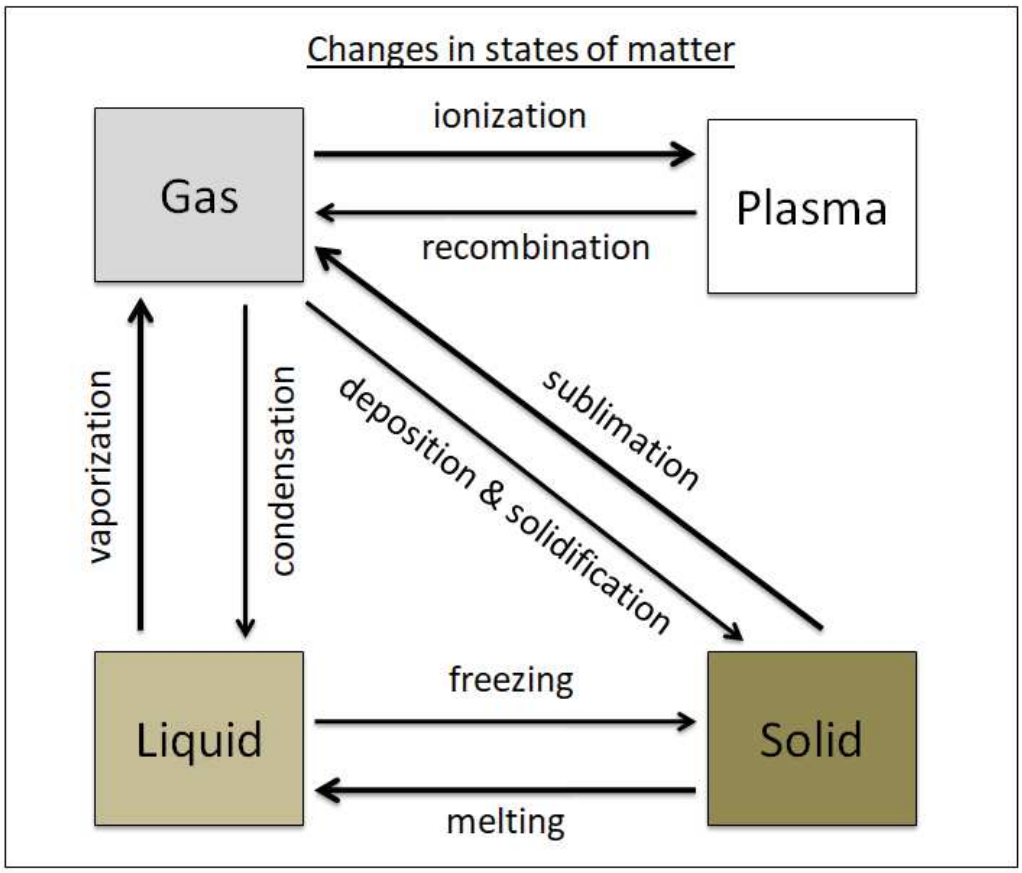

Fig. 1-1. Changes in the state of matter.

Figure 1-1 shows the changes in the state of matter by energy which mainly depends on the “temperature”. Thus, increasing the energy of solid phase will change solid to liquid phase through melting, or directly change solid to gas phase through sublimation. Likewise, increasing energy of liquid phase will change liquid to gas phase through vaporization. Moreover, increasing the energy of gas phase will ionize gas to plasma phase. On the other hand, reducing the plasma phase energy will change plasma to gas phase through recombination. Additionally, reducing the energy of gas phase will change gas to liquid phase through condensation or directly change gas to solid phase through deposition and solidification. Finally, reducing the energy of liquid phase will

change liquid to solid phase through freezing.

1.3 Coating using plasma

Plasma coating techniques have been developed over the years to conduct coating of high-quality functional films which are desired in many industrial fields. Plasma technology enables control of the coating processing with high accuracy in terms of thickness, morphology, hardness, etc. Furthermore, deposition, implantation and surface modification are important material processing for producing films on surfaces and modifying their properties. Film and mask deposition, mask patterning, implantation, other modification, etching and mask stripping are repeated many times during the manufacture of modern integrated circuit devices. Because device structures are sensitive to temperature, high temperature deposition processes cannot be used in many cases. Fortunately, owing to the non-equilibrium nature of low pressure processing plasma, films that are usually deposited at high temperatures can be deposited at low temperatures. Furthermore, films can be deposited with improved functional properties, non-equilibrium chemical compositions, and crystal morphologies that are unattainable under equilibrium deposition conditions at any temperature. Unique films like diamond not naturally found can be deposited [A6].

Sputtering process is generally accepted method for producing functional thin films by plasma. In the basic sputtering process, a target (or cathode) is bombarded by energetic ions generated in glow discharge plasma, situated in front of the target. The bombardment causes the removal or sputtering of target atoms, which may condense on a substrate as a thin film. At the same time, secondary electrons are emitted from the target surface as a result of the ion bombardment, and these electrons play important

roles to maintain plasma [A7]. Furthermore, there are many types of sputtering such as direct current (DC) sputtering, radio frequency (RF) sputtering, reactive sputtering and magnetron sputtering.

Sputtering deposition is a physical vapor deposition (PVD) method of thin film by sputtering, which is widely used in the thin film industry [A8]. This involves ejecting material from a "target" that is a source of thin film deposited onto a "substrate" such as a silicon wafer. In physical sputtering, incident ions physically sputter target atoms, which ballistically flow to a substrate and are deposited. Argon ions at 500-1000 eV are usually used for sputtering, which are suitable for sputtering almost all target materials including a very wide variety of pure metals, alloys, and insulators. Physical sputtering, especially of elemental targets, is a well-understood process, sputtering systems for various applications can be easily designed. Reasonable deposition rates with excellent film uniformity, good surface smoothness, and adhesion can be achieved over large areas. Refractory materials can also be easily sputtered. Sputtering deposition usually gives films with bad thickness uniformity, although re-deposition techniques by ion bombardment of the deposited film can improve the uniformity [A6].

Sputtering process is not commercially acceptable, because of its very low deposition rate. However, the use of magnetic field enhanced the sputtering process and led to the development of magnetron discharge which is widely used in many commercial applications owing to its high deposition rate [A9]. In magnetron sputtering, a magnetic field is used to sustain the discharge in the vicinity of the sputtered cathode (target). The magnetic circuit placed behind the sputtered cathode forms a tunnel of semi-toroidal magnetic field **B**. In this closed **B** field tunnel, plasma is confined and the sputtering gas is very efficiently ionized owing to a drift of electrons along the tunnel

axis in crossed **E** and **B** fields. This sputtering system is called the conventional magnetron (CM) system. The plasma of the CM is distributed in the vicinity of the sputtered target, where the magnetic field **B** is strongest [A10]. There are other types of magnetron systems: Unbalanced magnetron [A11], low-pressure magnetron [A12], magnetron with enhanced ionization [A13], ionized magnetron [A14], high-power and high-rate magnetron [A15], etc.

Moreover, magnetron sputtering has developed rapidly over the last decade and it has become the process for the deposition in a wide range of industrial coatings. The driving force behind this development has been the increasing demand for high-quality functional films in many diverse market sectors. In many cases, magnetron sputtered films now outperform films deposited by other physical vapor deposition (PVD) processes, and it can offer the same functionality as much thicker films produced by other surface coating techniques. Consequently, magnetron sputtering now gives a significant impact in application areas (e.g. wear-resistant coatings, low friction coatings, corrosion-resistant coatings, decorative coatings and coatings with specific optical or electrical properties).

On the other hand, magnetrons make use of the fact that a magnetic field configured parallel to the target surface can constrain electron motion in the vicinity of the target. The magnets are arranged in such a way in which one pole is positioned at the central axis of the target and the second pole is formed by a ring of magnets around the outer edge of the target. Trapping the electrons in this way substantially increases the probability of ionization by electron-atom collision. The increased ionization efficiency by magnetron results in a dense plasma at the target region. This leads to increased ion bombardment on the target, gives higher sputtering rates and higher deposition rates at

the substrate. In addition, the increased ionization efficiency achieved in the magnetron mode allows the discharge to be maintained at lower operating pressures (typically, 10^{-3} mbar, compared to 10^{-2} mbar) and lower operating voltages (typically, -500V, compared to -2 to -3 kV) [A7].

The evaporation and sputtering of solid materials are fundamental physical processes currently used in the physical vapor deposition (PVD) of thin films. The evaporation dominated over the sputtering for a very long time, and this was mainly due to a very low sputter deposition rate a_{Ds} ($1 \ll \mu$/min) of the film, and relatively high pressures p ($\geq$1 Pa) which is necessary to sustain sputtering discharge. The breakthrough was brought after the discovery of planar magnetron by Chapin [A16]. From that moment, sputtering method was developed rapidly. Furthermore, every important progress in magnetron technology depend on a deep understanding of the physical basis of magnetron discharges and on significant improvements of existing sputtering systems, as well as on the development of new systems operating under new physical conditions [A17].

1.4 Scope of this study

The purpose of this study is to develop new plasma coating methods of non-conductive films on inner and outer walls of non-conductive tubes. The coating process is relatively easier when the material of the tube substrate is electrically conductive. Furthermore, the coating process also depends on the coated film electrical properties. The coating process is relatively easier when the coated film is conductive as the coated film will play the role of an anode (extended anode effect). On the other hand, the coating process is very challenging when both the tube substrate and the coated film

are non-conductive. Therefore, the author investigates on new methods of coating of non-conductive films on inner and outer walls of non-conductive tubes.

1.5 Contents of this thesis

Chapter 1 contains background, and scope and purpose of this study. An introduction to plasma, sputtering process and magnetron discharges is also included in this chapter.

Chapter 2 contains “Advanced DLC coating technique for silicone-based tubular medical devices”. An advanced DLC coating technique has been developed to fabricate adhesive DLC layer on silicone-based tubular medical devices. The novelty of the multi-electrode coaxial magnetron plasma system includes the capability to produce a uniform and flexible DLC coating layer having high hardness and low friction coefficient by a hybrid technique of chemical vapor deposition (CVD) and physical vapor deposition (PVD). It is a simple single-step process such that pretreatment is not required on the silicone-based substrate. Furthermore, the deposited film was confirmed to be biocompatible.

Chapter 3 contains “Influence of physical conditions on extended anode effect in tube inner coating”. For uniform tube inner coating of non-conductive thin films, influence of physical conditions on extended anode effect on the double-ended coaxial magnetron pulsed plasma (DCMPP) method was examined. It was clearly shown that the extended anode effect was strongly influenced by the electrical resistance of the coated thin films on the inner surface of insulator tube. Additionally, high frequency (100 kHz) was better for relatively high plasma density and for avoiding the cathode cutting due to heat concentration. On the other hand, in the case of O_2 mixture, negative

ion production drastically decreased the deposition rate and increased the resistivity of coated TiO_2 films.

Chapter 4 contains “Tube inner coating of non-conductive films by pulsed reactive coaxial magnetron plasma with outer anode”. The double-ended coaxial magnetron pulsed plasma (DCMPP) method with an auxiliary outer anode (Aluminum) was developed in order to achieve uniform coating of non-conductive thin films on the inner walls of insulator tubes. It was clearly shown that using of an auxiliary outer anode with DCMPP enhanced the uniformity of the deposited film compared to DCMPP without outer anode.

In Chapter 5, major results are summarized. Then, the author concludes the study and refers to the outlook.

References

[A1] J. D. Callen, *Fundamentals of plasma physics*, Introduction, (E-book from University of Wisconsin, USA, 2006).

[A2] I. L. Němcová, *Study of plasma liquid interactions* (doctoral thesis, Brno University of Technology, Brno, Czech Republic, 2013), Chapter 1: Introduction.

[A3] F. F. Chen, *Introduction to plasma physics and controlled fusion, Volume 1: Plasma Physics* (1983), Chapter 1: Introduction.

[A4] O. Takai, Solution plasma processing, Pure Appl. Chem. **80**, 2011 (2003).

[A5] T. Shirafuji, Y. Himeno, N. Saito and O. Takai, Generation of Three-Dimensionally Integrated Micro Solution Plasmas and Its Application to Decomposition of Organic Contaminants in Water, J. Photopolymer Sci. and Tech. **26**, 507 (2013).

[A6] M. A. Lieberman, and A. J. Lichtenberg, *Principles of plasma discharges and materials processing*, (Second Edition, John Wiley & Sons Inc., 2004), Chapter 16: Deposition and implantation.

[A7] P. J. Kelly, and R. D. Arnell, Magnetron sputtering: a review of recent developments and applications, Vacuum **56**, 159 (2000).

[A8] T. Voutsas, H. Nishiki, M. Atkinson, J. Hartzell, Y. Nakata, Sputtering technology of Si films for low-temperature poly-Si TFTs, Sharp Technical Report, No.80 (2001) p.36.

[A9] S. Swann, Magnetron sputtering, Phys. Technol. **19**, 67 (1988).

[A10] J. Musil, S. Kadlec, Reactive sputtering of TiN films at large substrate to target distances, Vacuum **40**, 435 (1990).

[A11] B. Window, and N. Savvides, Charged particle fluxes from planar magnetron sputtering sources, Journal of Vacuum Science & Technology A: Vacuum, Surfaces, and

Films **4**, 196 (1986).

[A12] S. Kadlec, and J. Musil, Low pressure sputtering and self-sputtering, Vacuum **47**, 307 (1996).

[A13] J. Musil, S. Kadlec, and W. D. Munz, Unbalanced magnetrons and new sputtering systems with enhanced plasma ionization, J. Vac. Sci. Technol. **A9**, 1171 (1991).

[A14] C. Christou, and Z. H. Barber, Ionization of sputtered material in a planar magnetron discharge, J. Vac. Sci. Technol. **18**, 2897 (2000).

[A15] J. Musil, A. Rajsky, A. J. Bell, J. Matous, M. Cepera, J. Zeman, High rate magnetron sputtering, J. Vac. Sci. Technol. **14** , 2187 (1996).

[A16] J. S. Chapin, Res. / Dev. **25** (1), 37 (174); US Patent Appl. 438 (1974).

[A17] J. Musil, J. Vlcek, and P. Baroch, Magnetron Discharges for Thin Films Plasma Processing, *Materials surface processing by directed energy techniques* (Elsevier, 2006) Chapter 3.

Chapter 2

Advanced DLC coating technique on silicone-based tubular medical devices

2.1 Introduction

Recently, catheter and its guide wire are widely used for medical treatments. A catheter is a thin flexible pipe that is possible to be inserted into a body cavity, duct or vessel through the process of catheterization. Catheters enable administration and drainage of gases or fluids, and they allow the access of surgical equipment [B1]. The narrow and long metal wire guides a catheter to the affected part of human body. At present Ni-Ti alloy or stainless steel is used for the guide wire. For adding a biocompatibility and a low friction coefficient, the surface of the guide wire is coated by polyurethane and polytetrafluoroethylene (PTFE). These coatings have several problems such as peeling and abrasion. On the other hand, the catheter is required to exhibit higher biocompatibility. Therefore, diamond-like carbon (DLC) coating is very suitable for the items that are inserted into a human body, because DLC was approved to be biocompatible [B2].

DLC films have been coated by several methods such as direct ion beam deposition [B3], pulsed laser ablation [B4], ion beam conversion coatings [B5], filtered cathodic arc deposition [B6], plasma source ion implantation and deposition [B7], magnetron sputter coating [B8], and RF plasma-activated chemical vapor deposition [B9]. In this research, fine DLC coatings on medical-grade non-conductive silicone catheter for higher safety were investigated. Furthermore, the coating was carried out by multi-electrode coaxial magnetron plasma system utilizing a hybrid technique of

chemical vapor deposition (CVD) and physical vapor deposition (PVD) as illustrated in Fig. 2-1. Here hybrid means that both CVD and PVD techniques were combined together. Carbon atoms are sputtered by ionized argon gas and deposited on the surface of the substrate (PVD process) [B10]. On the other hand, thin films are deposited on a substrate surface through the chemical reactions of gaseous molecules which contain the atoms that are desired to form the deposited film (CVD process). These chemical reactions generally occur on the surface of the substrates and it is also possible to take place in the gas phase [B11]. In this study the CVD was performed using reactive carbon source gases.

The DLC coatings on silicone-based catheter were performed by multi-electrode coaxial magnetron plasma system. The coatings showed the potential use of DLC coating on silicone catheters. Therefore, it was revealed that the multi-electrode coaxial magnetron plasma system was valid for the coating of non-conductive films on the outer wall of non-conductive narrow tube.

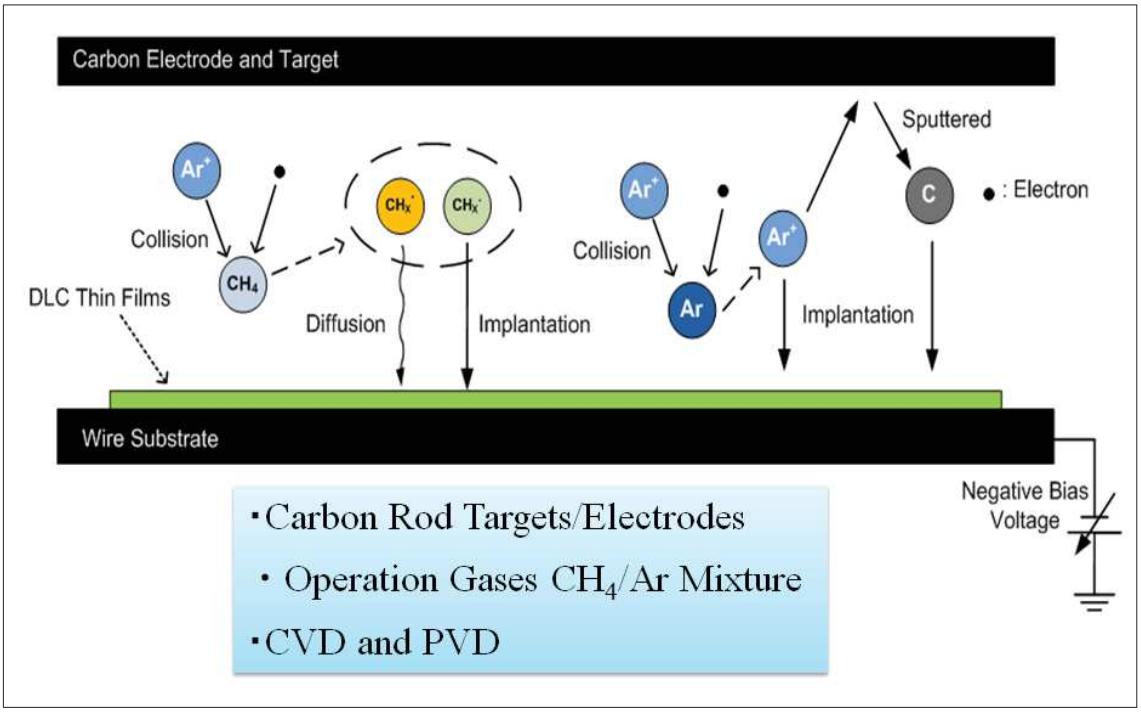

Fig. 2-1. CVD&PVD Hybrid Coating technique.

2.2 Experimental methods

2.2.1 Coaxial magnetron plasma with multiple electrodes system and experimental conditions

The experimental system utilizing coaxial magnetron plasmas with multiple electrodes is shown in Figs. 2-2. The silicone-based tubular medical device (catheter) having an outer diameter of 2 mm and a length of 270 mm was located at the center of four carbon electrodes (target cathode). A negative pulse bias voltage of -100 V was applied to the wire positioned inside the substrate, and a negative DC high voltage was applied to carbon electrodes that were surrounded by eight aluminum rods, as shown in Fig. 2-2(a). The electric fields around the electrodes are illustrated in Fig.2-2 (b).

Detailed diagram of the experimental system is shown in Fig. 2-3. The electrode system shown in Fig. 2-2 was located in a cylindrical chamber on which solenoid coil

was wound for axial magnetic field application. Ar and C_2H_2 were the gas species used in the reaction. A hybrid technique of plasma-enhanced chemical vapor deposition (PECVD) and physical vapor deposition (PVD) was used to carry out DLC deposition. The experimental conditions are shown in Table 2-1. The DLC-coated silicone-based tubes were characterized by optical microscopy, Raman scattering spectroscopy, and stretching/frictional wear tests. The friction test conditions are shown in Table 2-2. The tubes were further observed in cell culture with adipocytes of mouse to verify their biocompatibility. The results were compared with the uncoated tube.

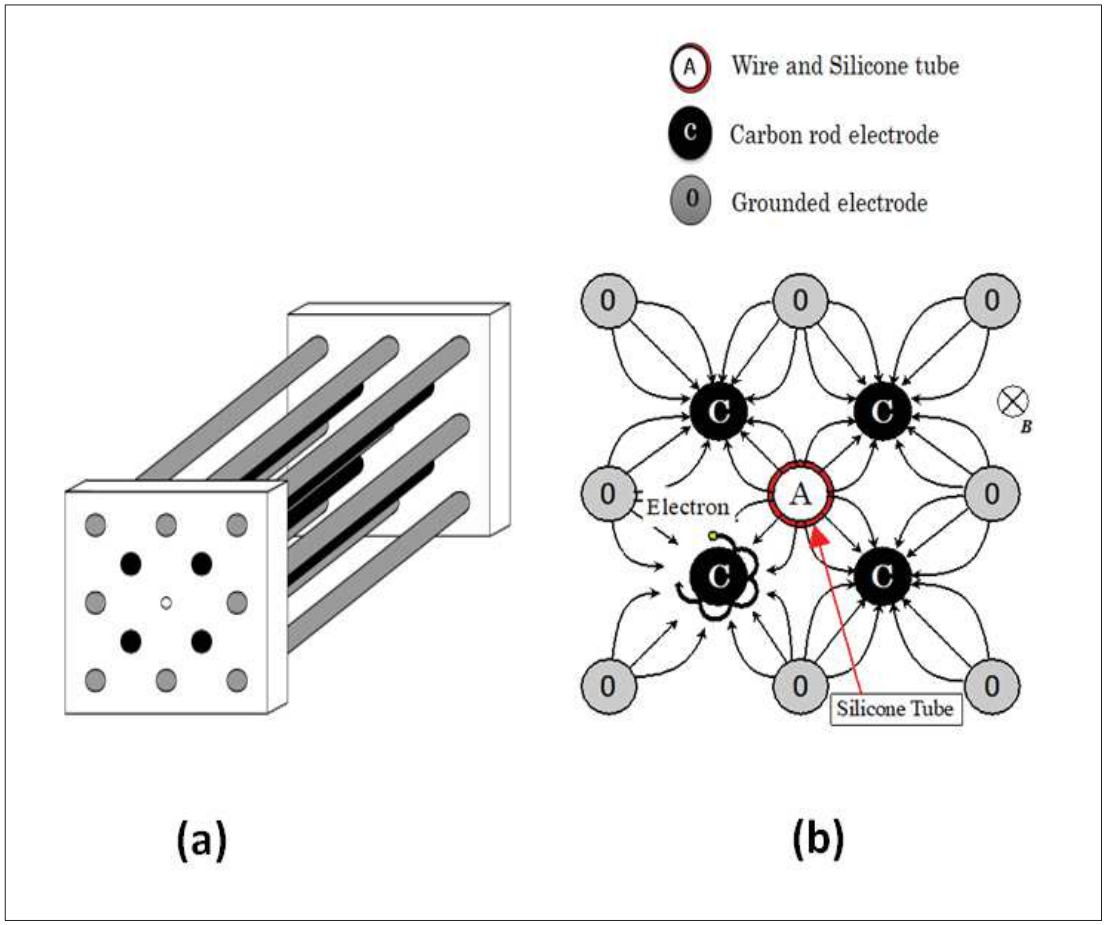

Fig. 2-2. Configuration of electric field of coaxial magnetron plasmas with multiple electrodes and its holder. (a) Electrode holder, and (b) electric field.

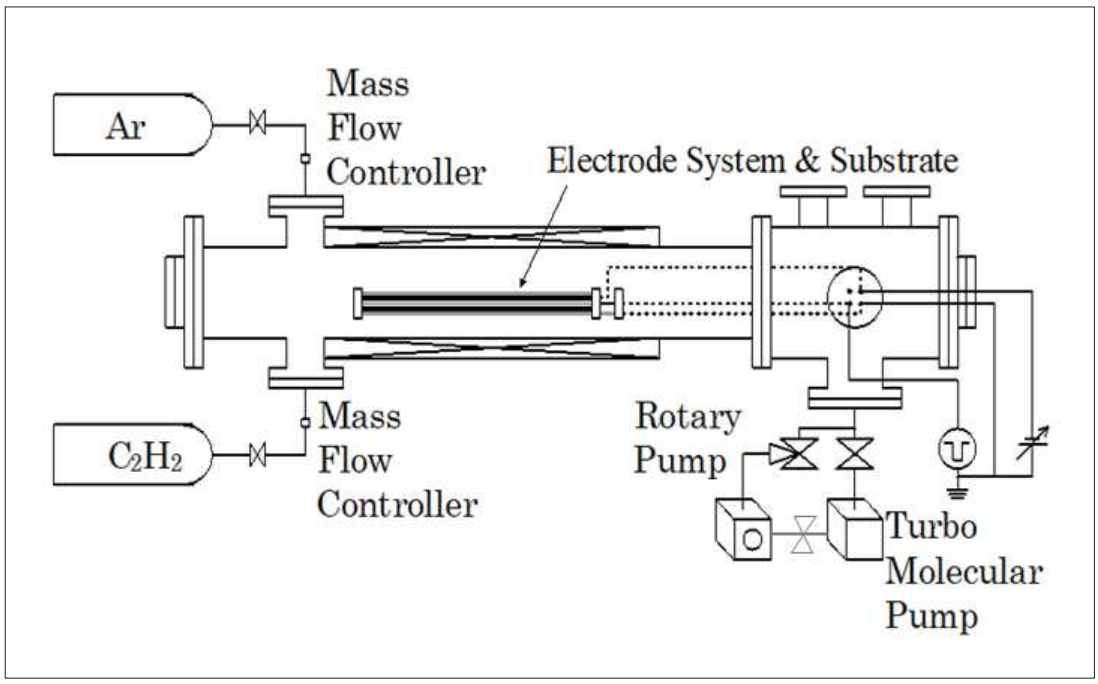

Fig. 2-3. Experimental apparatus of coaxial magnetron plasmas with multiple electrodes.

Table 2-1. Experimental condition.

Deposition Method	CVD&PVD
Gas Pressure [Pa]	10
Magnetic Flux Density [Gauss]	250, 300, 350, 400
Discharge Voltage [V]	-400
Substrate Repetition Pulse Bias Voltage [V]	-100
Pulse Repetition Frequency [kHz]	1
Duty Ratio [%]	50
Deposition Time [min.]	60

Table 2-2. Experimental conditions of friction test.

Test load	490 [mN]
Length of Stroke	4 [mm]
Frequency	2 [Hz]
Cycle	1200

2.2.2 Verification of biocompatibility

Cell line (MC3T3-E1, Riken Cell Bank was used for in-vitro evaluation of the DLC coated catheter. α-MEM (MEM Alpha; GIBCO, Invitrogen) containing 10% fetal bovine serum (GIBCO) and 1% antibiotic, 100 units per mL penicillin and 100 µg per mL streptomycin (GIBCO) was used as a plane medium for cell morphology and viability test. Frozen cells were heated for 1 min at 37 °C and cells were dispersed in medium and kept in a humidified CO_2 incubator at 37 °C. Cells were proliferated for 5 days and were detached by 0.25% trypsin (GIBCO). Detached cells were used for making the cell suspension with 1×10^4 cells per cm^2. The cells were seeded on the samples and the culture medium was changed every 2 days. Each experiment was performed in quadruple (n= 4) for each group of samples.

a) Cell morphology

A cell suspension, 1×10^5 mouse adipocyte cells per well, was cultured on the sample for 3 hours to observe morphology of the cells. Before fixation the cells were rinsed gently with a PBS (−) solution. 2.5% glutaraldehyde (Wako) was used for fixation of cells. The cells after fixation at 4 °C for 2 hours were dehydrated using upgrade ethanol, at the final step of dehydration, the samples were kept in 100% ethanol at room temperature for 30 min which followed drying at room condition. Finally dried samples were coated with gold by sputtering for SEM observation and photography.

b) Cell viability

By culturing undifferentiated mouse osteoblastic MC3T3-E1 cells on the sample surfaces, verification of cell viability was performed. MC3T3-E1 osteoblasts were maintained at 37 °C in medium (5% humidified CO_2). The one solution cell proliferation assay (CellTiter 96® AQueous, MTS assay, Promega Corp. [B12] was

used for cell viability evaluation. MTS assay was added to MC3T3-E1 cells at days of 2nd, 4th, and 6th after 4-hour incubation at 37 °C atmosphere of 5% CO_2. The solution was taken from all wells and the solution was transferred into each well of 96-well plates and their absorbance at 490 nm was obtained.

2.3 Results and discussion

2.3.1 Mechanical property of DLC coated silicone tube

According to the Child-Langmuir Law in a magnetic field [B13] the discharge current I_d is given by:

$$I_d = A(aP^2 + bB^2)(V_d - V_0)^{3/2}, \quad (2\text{-}1)$$

where, P is the pressure, B is the magnetic flux density, V_d is the discharge voltage, V_0 is the breakdown voltage, and A, a, and b are the constants of proportionality. Therefore, I_d is proportional to the 3/2 power of the discharge voltage, and it is proportional to a square of the pressure and the magnetic flux density. As observed in Fig. 2-4, the current density increases with increasing magnetic flux density.

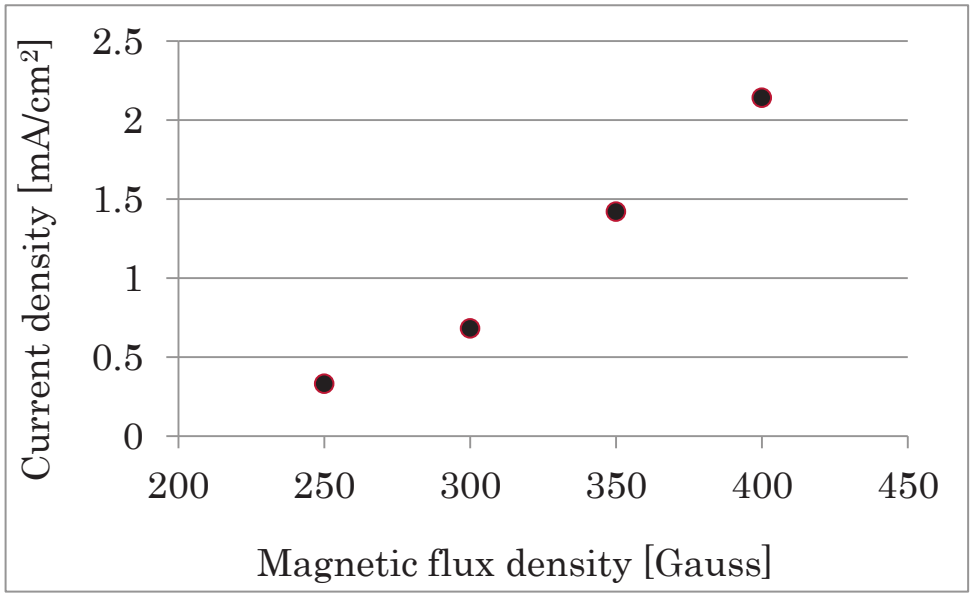

Fig. 2-4. Current density as a function of magnetic flux density.

As it is possible to obtain the ratio of sp2 to sp3 by measuring the ratio of the stretching mode to the breathing modes of sp2 bonds, DLC film was observed by Raman scattering spectroscopy which are shown in Fig. 2-5. D and G peaks appeared in the vicinity of 1350 cm^{-1} and 1590 cm^{-1}, respectively. The G peak corresponds to the bond stretching of all pairs of sp^2 atoms and the D peak corresponds to the breathing modes of sp^2 atoms. These peaks were confirmed in all the samples in this study. D peak becomes conspicuous when current density increases. Therefore, the deposited film was supposed to be DLC at the lower current density.

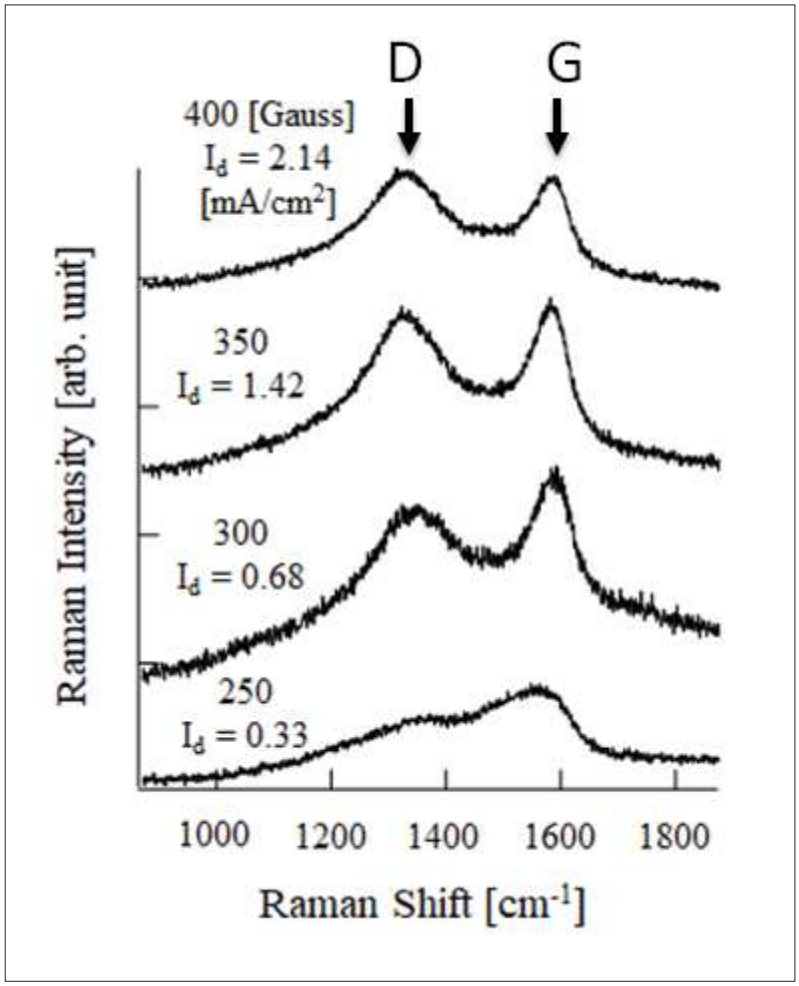

Fig. 2-5. Variation of Raman Spectrum due to increase in flux density.

Moreover, ID/IG ratio is plotted from each Raman spectrum as shown in Fig. 2-6. The increase of the ID/IG ratio is in accordance with the increase of the plasma density. The ratio is said to be derived from the grain size of carbon film [B-14]. High plasma density increases the size of carbon crystallites, while low plasma density decreases the carbon crystallites size.

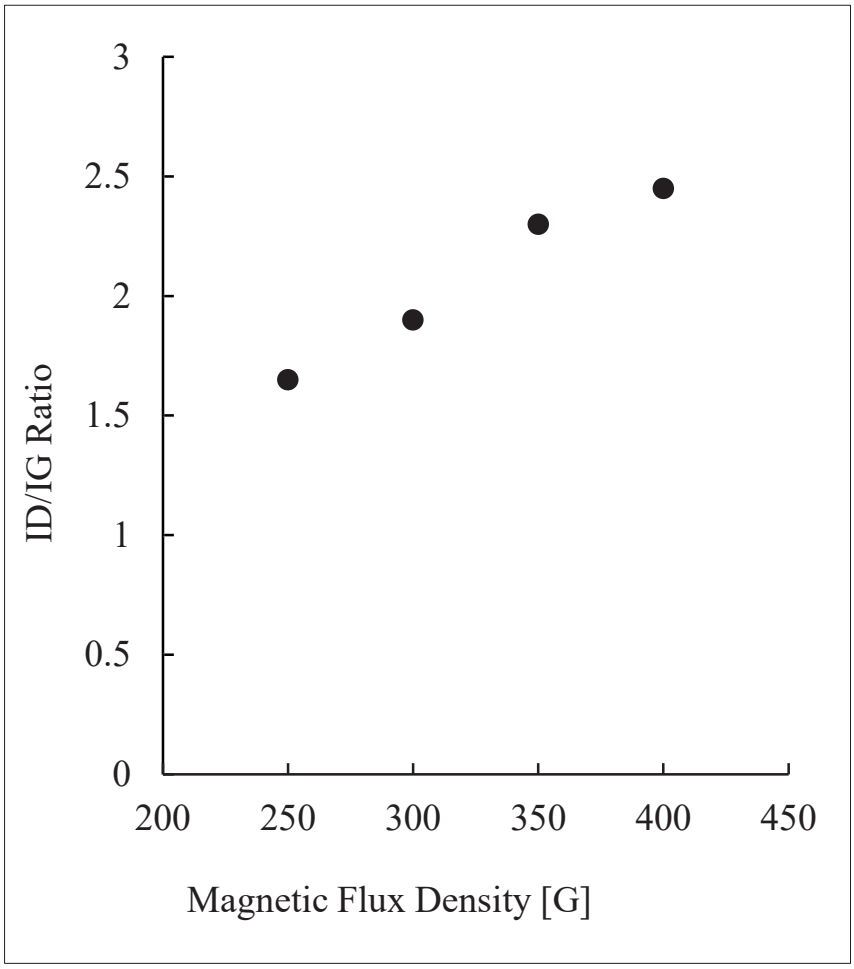

Fig. 2-6. ID/IG ratio of coated DLC as a function of magnetic flux density.

The results of friction coefficient test are shown in Fig. 2-7. The test was performed by a pin-on-disc type system under the conditions in which test load was 490 mN, rotation speed was 120 rpm, and rotation number was 1200 times. More detailed test conditions are shown in Table 2-2. Friction coefficients of the DLC prepared at magnetic flux density of 250 G and 350 are 0.1 and 0.2, respectively, which is about 1/5 of the uncoated reference. However, the friction coefficient in accordance with the number of cycles increased. The possible explanation is the membranaceous change that is related to the carbon crystallites size in the DLC film. It was observed that the

(ID/IG) ratio tends to increase with increasing the strength of the magnetic flux density under the experimental conditions. This is due to carbon crystallite size [B15]. That is, increasing magnetic flux density will increase the carbon crystallite size which will lead to formation of rough DLC with high friction coefficient. On the other hand, decreasing the magnetic flux density will decrease the carbon crystallite size which will lead to formation of smooth DLC with low friction coefficient.

Coating of DLC film with thickness of 3 μm was achieved under the optimum conditions. The deposited film exhibited high hardness, good adhesion, and low friction coefficient.

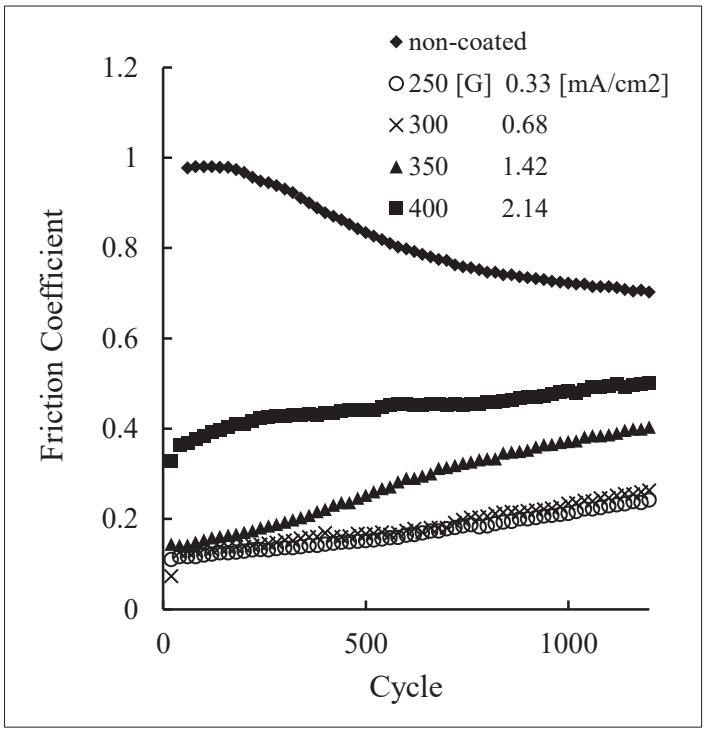

Fig. 2-7. Friction coefficient as a function of cycle.

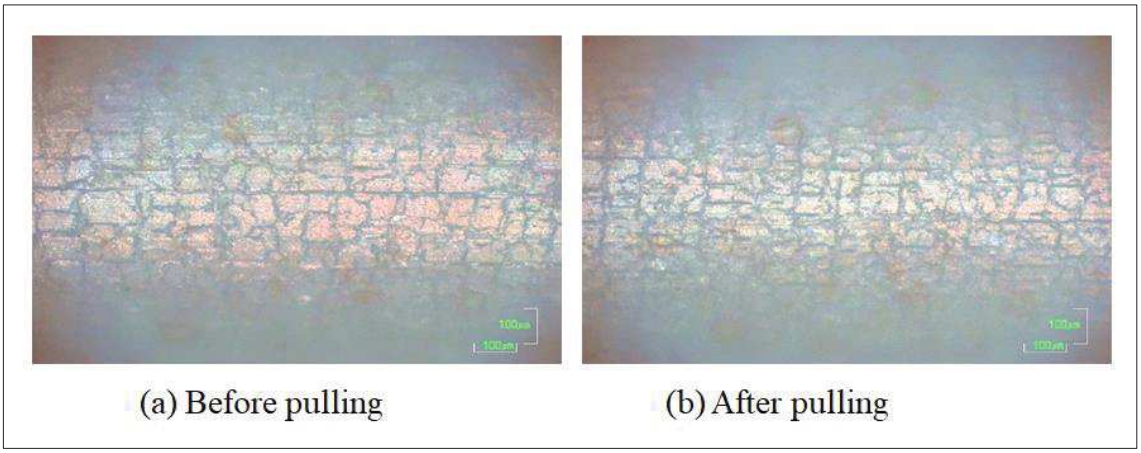

Fig. 2-8. Coated silicone tube (a) before, and (b) after pulling.

Figure 2-8 shows results of the stretching test of the coated silicone tube of 20 mm length before stretching, then the tube was stretched for 10 mm and the results showed no sign of DLC peeling off.

2.3.2 Cell morphology

The evaluation of the direct contact between cells and biomaterials identifies the presence of potential leachable. In pilot experiment, biocompatibility of the silicone catheter was assessed. Preliminary results indicate that mouse adipocytes were viable on both uncoated and DLC coated silicone surfaces 6 days after the initial contact. Cell viability on DLC coated tubes is required to show that the new coating is not toxic and viability is at least in the level of untreated sample.

In pilot experiment, biocompatibility of the silicone was assessed by SEM images of cells morphology after 4-hour cell culture and incubation. Fig. 2-9 shows the cell morphology result with mouse adipocyte cells and indicates that no toxicity was shown in both uncoated (a) and DLC coated silicon surfaces (b) after 4-hour initial contact. The result revealed that attachment and extension of cells after 4-hour cell cultures were

totally different between DLC coated and uncoated silicone surfaces. In cells exposed to bared silicone surface, altered cell morphology with rounding and partial detachment appears, while cells exposed to DLC coated surface maintain typical filopodial shape and well expansion. The surface was also covered by extra cellular matrix even after 4-hour cell culture. Untreated and treated samples show totally different topologies. Therefore, the cell morphology on DLC-coated samples shows to be similar to the surfaces with similar topology. Although the cell morphology of the DLC coated silicone was affected by nanoscale surface topology change after the surface coating, the cells were well spread on the surface regardless of the deposited carbon film characteristics or wettability of the surface.

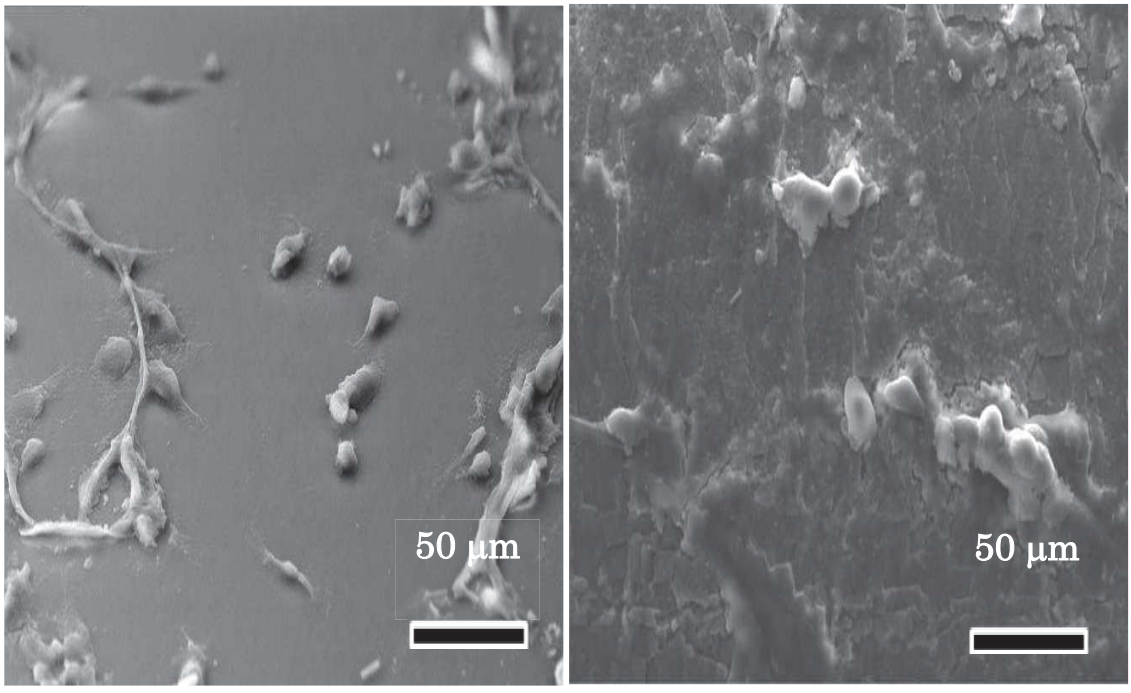

(a) uncoated surface (b) DLC

Fig. 2-9. SEM photographs of adipocyte cells on (a) uncoated surface and (b) DLC coated silicone tube surface.

2.3.3 Cell viability

Figure 2-10 shows the cell viability on DLC coated and uncoated silicone tubes quantified by the MTS assay after culturing for 2, 4 and 6 days. The level of cell growth was not significantly higher on the DLC coated silicone tube after 4-day and 6-day cell culture compared to untreated silicone tube. The cell proliferation results culturing for 4 and 6 days clearly demonstrate that cells were viable on both untreated and DLC-coated silicone tubes and that there is no toxic effect of the DLC coated silicon on the cell attachment, growth and proliferation stages.

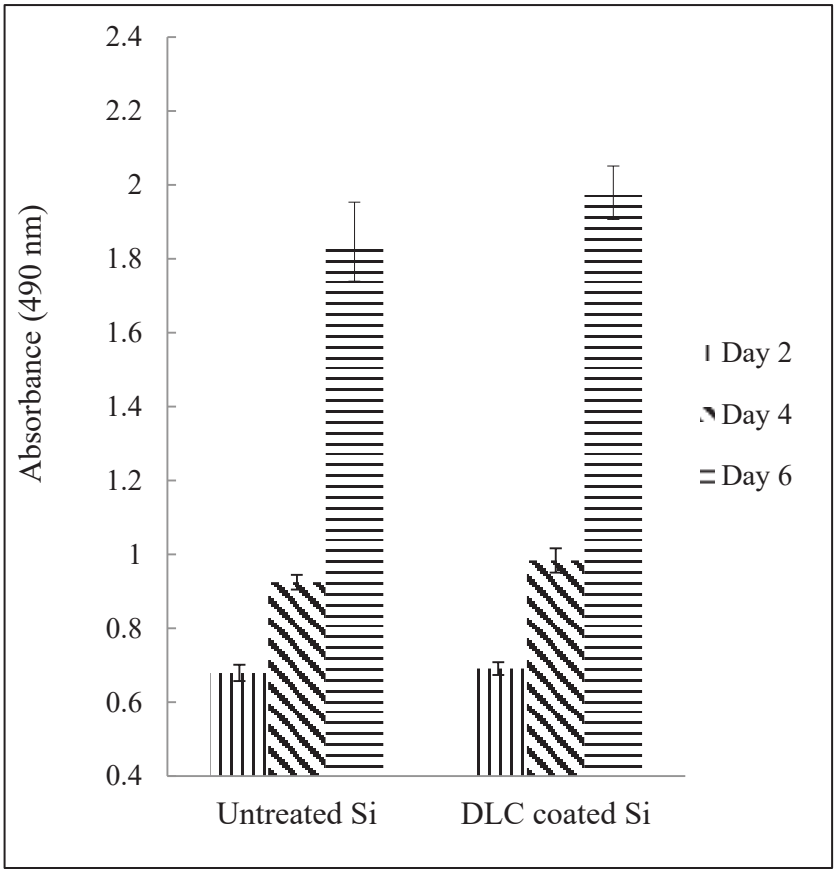

Fig. 2-10. Cell viability bar graph for untreated silicone and DLC coated silicone.

2.4 Brief summary

DLC coating on flexible silicone tube has been prepared by the coaxial magnetron plasma with multiple electrodes [B16]. Raman data indicated the presence of DLC, and the influence of plasma density on the size of carbon crystallites. Low friction-coefficient DLC was obtained at low magnetic flux density. Preliminary cell culture results verify that DLC coatings on silicone surface are biocompatible. From the above, co-axial magnetron plasma with multiple electrodes (ground electrodes and targets) is revealed to be useful for DLC coating on the outer wall of non-conductive narrow tube (e.g. catheter).

References

[B1] R. C. Diggery, D. T. Grint, *Catheters: types applications and potential complications* (Nova Biomedical, 2012) Introduction.

[B2] G. Dearnaley, J. H. Arps, Biomedical applications of diamond-like carbon (DLC) coatings: a review, Surf. Coat. Technol. **200**, 2518 (2005).

[B3] Y. Liu, A. Erdemir, E. I. Meletis, A study of the wear mechanism of diamond-like carbon films, Surf. Coat. Technol. **82**, 48 (1996).

[B4] A. A. Voevodin, M. S. Donley, J. S. Zabinski, Pulsed laser deposition of diamond-like carbon wear protective coatings: a review, Surf. Coat. Technol. **92**, 42 (1997).

[B5] C. G. Fountzoulas, T. Z. Kattanis, J. D. Demaree, J. K. Hirvonen, in: A. Feldman, Y. Tzeng, W. A. Yarbrough, M. Yoshikawa, M. Murakawa (Eds.), *Applications of diamond films and related materials: third international conference* (Special Publication 885, National Institute of Standards and Technology, USA, 1995) p.907.

[B6] S. Xu, B. K. Tay, H. S. Tan, L. Zhong, S. R. F. Silva, W. I. Milne, Properties of carbon ion deposited tetrahedral amorphous carbon films as a function of ion energy, J. Appl. Phys. **79**, 7234 (1996).

[B7] S. Anders, A. Anders, I. Brown, F. Kong, F. McLarnon, Surface modification of nickel battery electrodes by cobalt plasma immersion ion implantation and deposition, Surf. Coat. Technol. **85**, 75 (1996).

[B8] X. L. Peng, Z. H. Barber, T. W. Clyne, Surface roughness of diamond-like carbon films prepared using various techniques, Surf. Coat. Technol, **138**, 23 (2001).

[B9] A. Erdemir, I. B. Nilufer, O. C. Eryilmaz, G. R. Fenske, Friction and wear performance of diamond-like carbon films grown in various source gas plasmas, Surf.

Coat. Technol. **120/121**, 589 (1999).

[B10] T. Voutsas, H. Nishiki, M. Atkinson, J. Hartzell, Y. Nakata, Sputtering technology of Si films for low-temperature poly-Si TFTs, SHARP Tech. J. **80**, 36 (2001).

[B11] H. Pedersen and S. D. Elliott, Studying chemical vapor deposition processes with theoretical chemistry, Theoretical Chemistry accounts **133**, 1476 (2014).

[B12] T. C. Owen, A. H. Cory, J. G. Cory, J. A. Barltrop, 5-(3-carboxymethoxyphenyl)-2-(4,5dimenthylthiazoly)-3-(4-sulfophenyl)tetrazolium, inner salt (MTS) and related analogs of 3-(4,5 dimethylthiazolyl)-2,5-diphenyltetrazolium bromide (MTT) reducing to purple water soluble formazans as cell-viability indicat, Bioorg. Med. Chem. Lett. **1**, 661 (1991)

[B13] K. Kuwahara, H. Fujiyama, Application of the Child-Langmuir law to magnetron discharge plasmas, IEEE Trans. Plasma Sci. **22**, 442 (1994)

[B14] J. Robertson, Diamond-like amorphous carbon, Mater. Sci. Eng. **37**, 129 (2002).

[B15] Y. Yoshimura, K. Yamanouchi, Study on DLC thin film deposition technology using sputtering for a semiconductor component, Kagoshima Prefectural Institute of Industrial Technology **26**, 65 (2012).

[B16] M. T. I. Gasab, M. Uchiyama, T. Nakatani, A. Valanezhad, I. Watanabe, H. Fujiyama, Advanced DLC coating technique on silicone-based tubular medical devices, Surf. Coat. Technol. **307**, 1084 (2016).

Chapter 3

Influence of physical conditions on extended anode effect in tube inner coating

3.1 Introduction

Narrow tubes are commonly and widely used in industry to deliver water, gas, cooling substances, etc. [C1]. However, these tubes are often required to have excel performances in terms of corrosion and wear resistance. It is, therefore, necessary to create protection films on the inside walls of tubes. In this regard, several studies have been conducted [C2-C10]. In addition, sputtering method using coaxial magnetron pulsed plasma (CMPP) has been proposed by H. Fujiyama *et al*. for inner narrow tube coating [C10, C11]. In the sputtering process using CMPP, plasma must be shifted along the tube. Shifting of plasma can be caused by a fact that the deposited conductive film plays a role of anode. This is the extended anode effect, which is effective in the conductive film coating. The shifting velocity was reported to increase with sputtering yield of the target material and to decrease with the electric resistivity of the deposited film [C10, C11]. The shifting velocity also depends on the properties of the target materials (cathode). As many physical parameters affect the extended anode effect, further studies on the effects of physical conditions are required.

In the present study the author investigated the extended anode effect for titanium-oxide (TiO_2) and titanium-nitride (TiN) films that have different electric resistivity. Furthermore, the author discussed the influence of the physical conditions on the extended anode effect from the viewpoints of electric resistivity and oxygen negative ions.

3.2 Experimental method

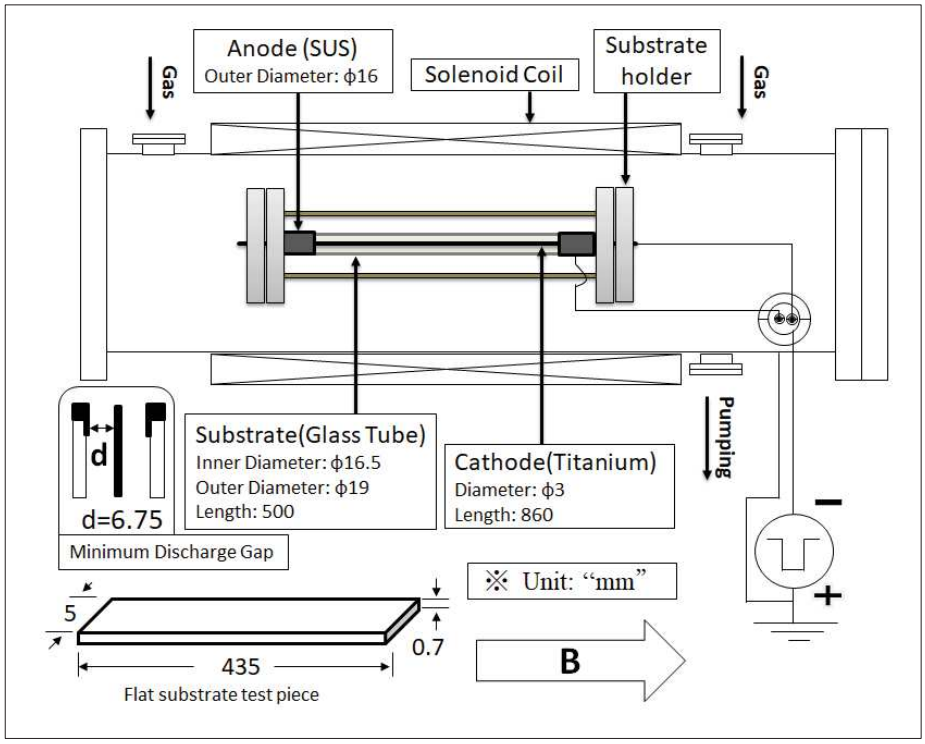

Fig. 3-1. Experimental apparatus.

Figure 3-1 shows the experimental equipment for tube inner coating by double-ended coaxial magnetron pulsed plasma (DCMPP). A long cylindrical vacuum chamber of 1300 mm in length and 320 mm in inner diameter was used. Water-cooled solenoidal coil was arranged coaxially around the chamber. DCMPP electrode was placed inside the chamber. Pulsed discharge took place between the long narrow cathode (titanium rod of 3mm in diameter) and the grounded anode. The anode consisted of two connected parts. The first part was short stainless steel (SUS) ring at both sides of the tube (16 mm in outer diameter), and the second part was glass tube (19 mm in outer diameter, 16.5 mm in inner diameter, and 500 mm in length). However, the

coated part of the glass tube was only 435 mm in the middle of the tube, since the uncoated parts at both edges of the glass tube were covered by the two SUS ring anodes.

Axial strong magnetic field (833 Gauss) was applied. Owing to the magnetron effect the breakdown can be made easier in a narrow tube under low-pressure conditions than without axial magnetic field. Coating was performed in argon and nitrogen mixture ($Ar+N_2$) as well as argon and oxygen mixture ($Ar+O_2$) gas. Discharge onset pressure was investigated in the range of 0.5~2.5 Pa, and optimum discharge pressure was determined to be 1 Pa according to Paschen curve. The detailed experimental conditions are shown in Table 3-1.

In order to evaluate the thickness of the coated films, a flat glass substrate test piece (435 mm in length and 5 mm in width and 0.7 mm in thickness) was inserted inside the tube as shown in Fig. 3-1. The flat substrate was marked by a magic pen at several positions. The mark plays a role which prevents coating and makes a step change in the film thickness at the positions marked. We evaluated the thickness of coatings by measuring the height of the step change at the corresponding position with a surface profilometer (Veeco dektak 150). After the measurement of film thickness, the flat substrate was cut into several pieces at the points that were marked by the magic pen. Then, the electrical resistance R was measured by contacting ohmmeter probes at the edges of both ends of a cut piece. Consequently, the resistivity ρ was calculated by the formula,

$$\rho = RA/L \qquad (3\text{-}1)$$

where, L and A are the distance between the probes, and the cross sectional area of the film, respectively.

Table 3-1. Experimental conditions.

Magnetic flux density [Gauss]	833
Gas pressure [Pa]	1
Mass flow rate of Ar [SCCM]	100, 90, 80, 70, 60, 50
Mass flow rate of N_2 [SCCM]	0,10,20,30,40,50
Mass flow rate of O_2 [SCCM]	0,5,10,15,20,25
Applied power [Watt]	300
Duty cycle [%]	55
Pulse repetition frequency [kHz]	100
Sputtering time [min]	2 (15 sec×8)

3.3 Results and discussion

3.3.1 Influence of pulse repetition frequency

Figure 3-2 shows the waveforms of discharge current (I_d) and voltage (V_d). The pulsed voltage was generated with a power supply (Advanced Energy, Pinnacle Plus+ 10 kW (325-800 V dc)), and the current was measured with a Rogowski coil and an oscilloscope. Plasma is produced soon after the voltage drop, and ends within a few μs which is shorter than the duration of the on-time. The negative charges flow to anode (glass tube), while positive charges flow to cathode (target). As a result, negative

charges are accumulated on the inner walls of glass tube. When the coated film is conductive, accumulated charge will be relaxed. However, the relaxation effect is not effective for non-conducting film. The accumulated charge in the glass tube will be also relaxed with the residual space charge. They will be driven by the inverse field caused by the accumulated charge. The inverse current during the off-time in Fig. 3-2 may suggest the relaxation effect of the space charge.

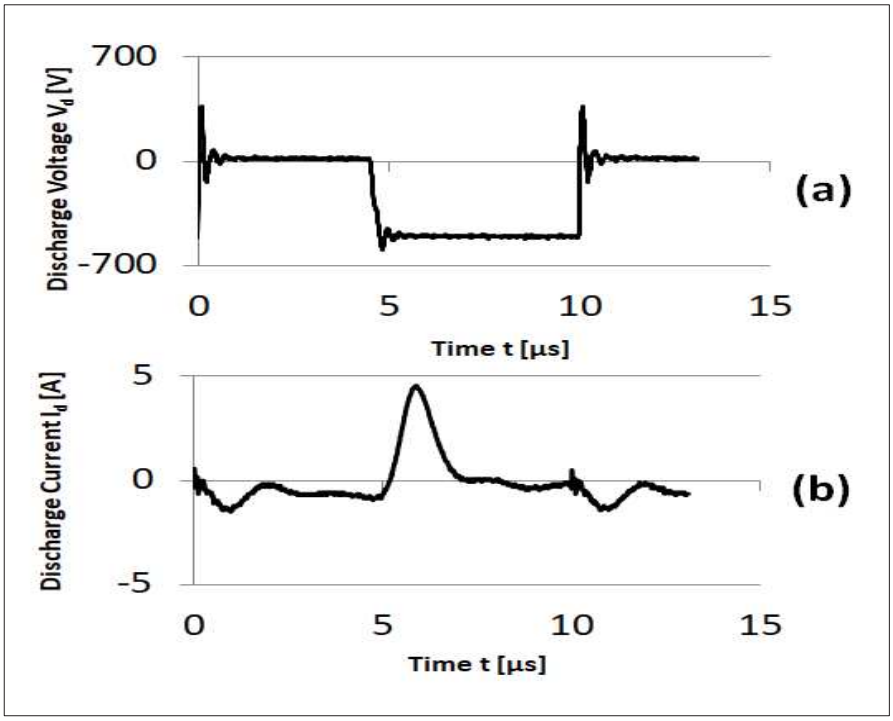

Fig. 3-2. Waveforms of (a) Discharge voltage (V_d) and (b) Discharge current (I_d).

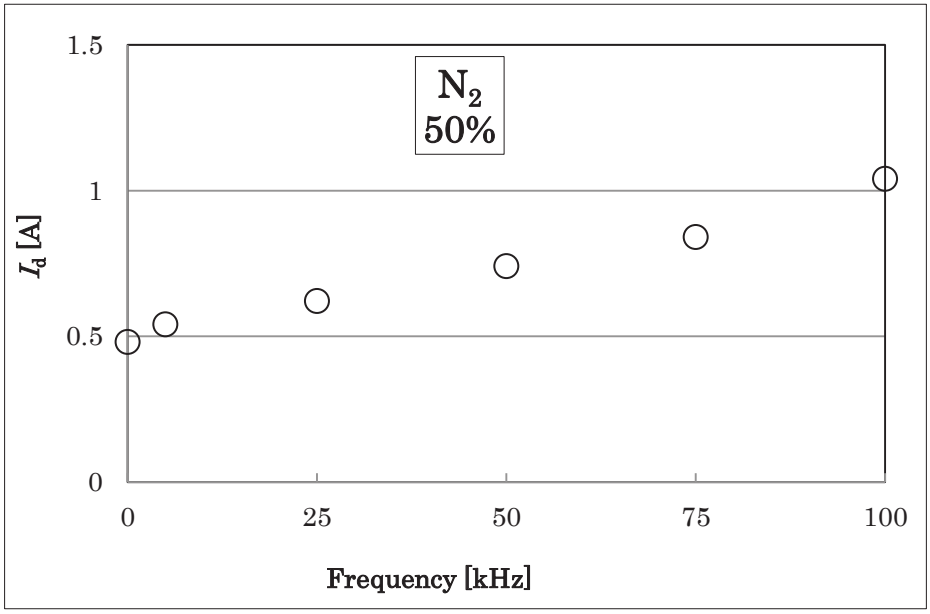

Fig. 3-3. Discharge current (I_d) as a function of pulse repetition frequency.

Based on the results in Fig. 3-2, the influence of the pulse repetition frequency was examined. Fig. 3-3 shows the discharge current (I_d) as a function of the pulse repetition frequency of the applied voltage. The current I_d increased with the frequency. Therefore, it was better to use high frequency (100 kHz).

3.3.2 Influence of nitrogen fraction

The effect of N_2 fraction in the gas mixture (f_{N2}) on discharge current (I_d) and discharge voltage (V_d) were observed with an oscilloscope and the monitor of the power supply. Fig. 3-4 shows the discharge voltage and discharge current as a function of fraction of N_2. Under the constant power, the discharge voltage V_d increased and the discharge current I_d decreased with increasing of f_{N2} as shown in Figs. 3-4 (a) and (b).

Figure 3-5 shows the film thickness as a function of fraction of N_2. Fig. 3-5 clearly shows that the film thickness decreased with f_{N2}.

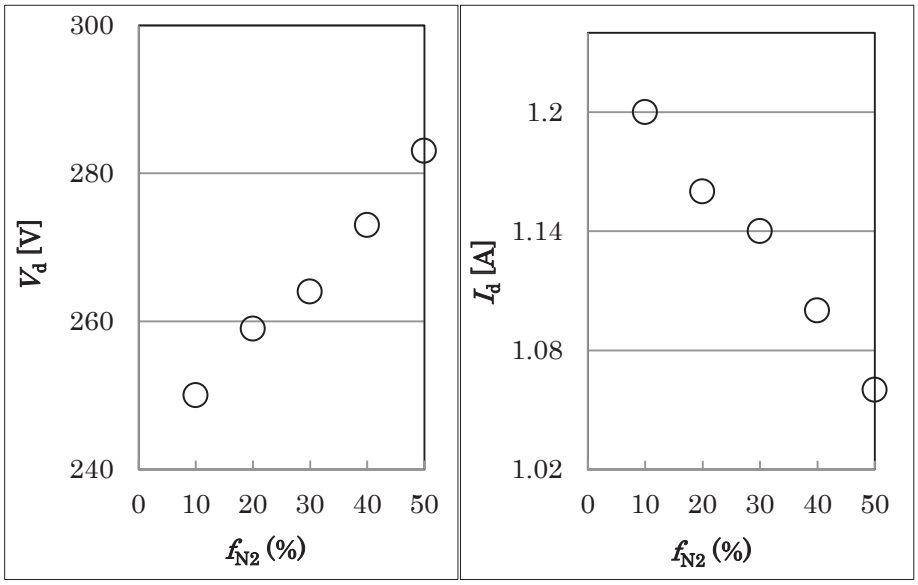

(a) discharge voltage (b) discharge current

Fig. 3-4. Discharge voltage and discharge current as a function of fraction of N_2.

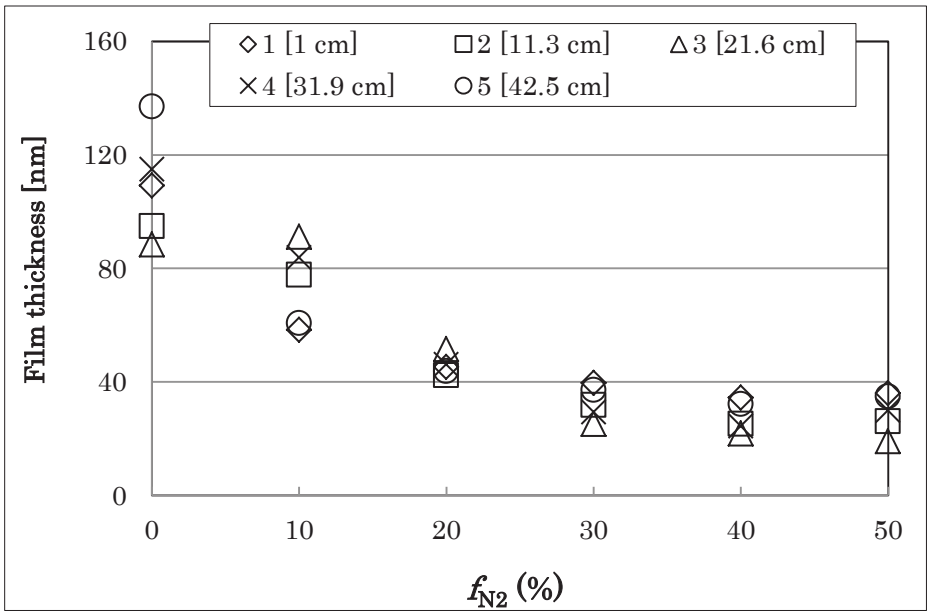

Fig. 3-5. Film thickness as a function of fraction of N_2.

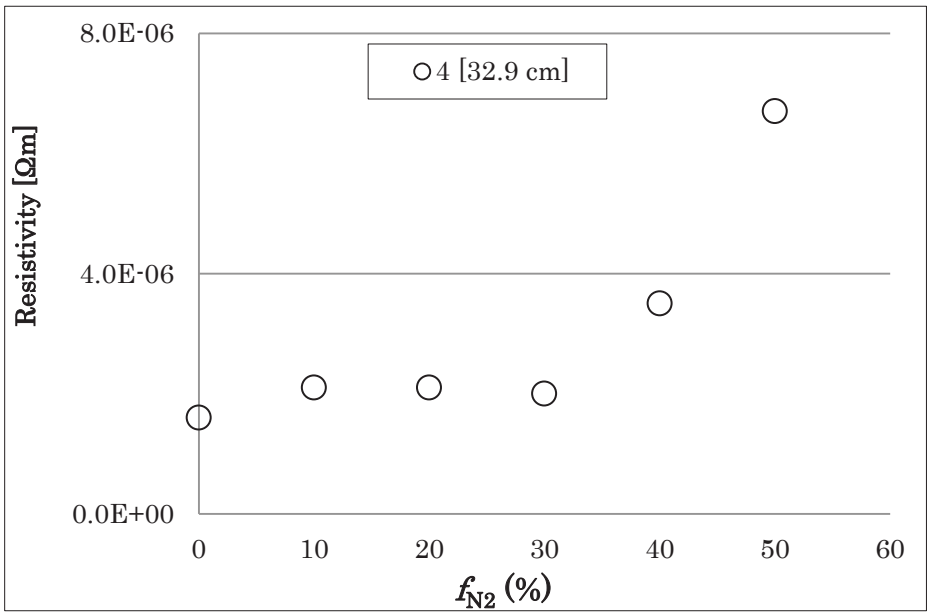

Fig. 3-6. Film resistivity as a function of fraction of N_2.

Figure 3-6 shows the film resistivity as a function of fraction of N_2. The film resistivity increased with f_{N2} when f_{N2} was more than 30%. At this point, the deposited film is supposed to be changed from metallic titanium to titanium-nitride (TiN). The reason why the thickness decreased with f_{N2} shown in Fig. 3-5 can be attributed to the increase of the film resistivity and the change of deposited film.

3.3.3 Influence of oxygen fraction

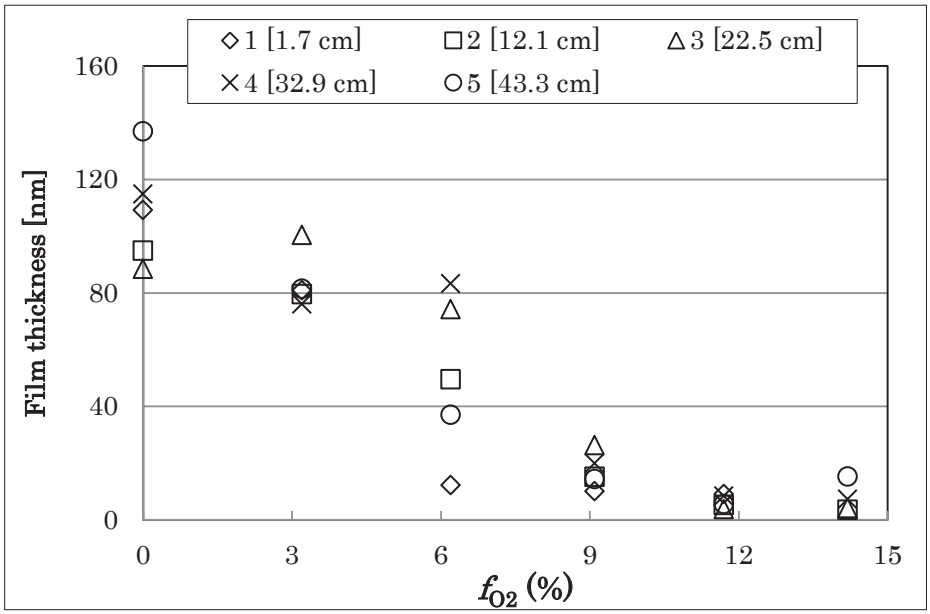

Fig. 3-7. Film thickness as a function of fraction of O_2 for different axial positions along the tube.

It was found that film thickness decreased with fraction of O_2 (f_{O2}) increased as shown in Fig. 3-7. In the case of TiO_2 inner coating, both of negative ion production and electrical resistance would strongly influenced on the extended anode effect. Here, to compare TiO_2 coating with other coating in which negative ions are not produced, TiN coating was performed.

Figure 3-8 shows the film resistivity as a function of fraction of O_2 (f_{O2}). The electric resistivity of deposited film increased with f_{O2} and became very large at f_{O2}=9.1 (%). This result is supposed to be due to the formation of TiO_2 film instead of Ti film.

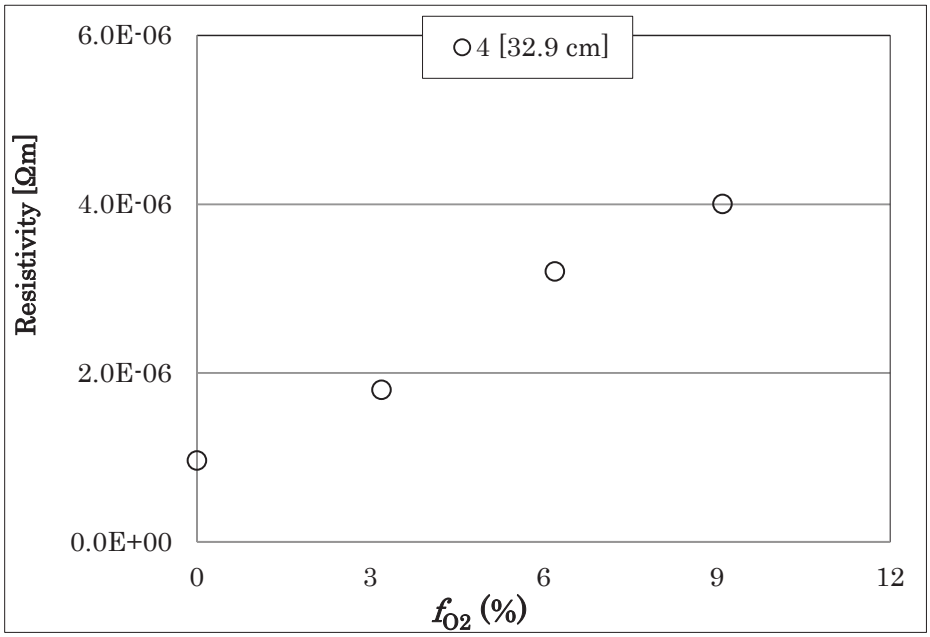

Fig. 3-8. Film resistivity as a function of fraction of O_2.

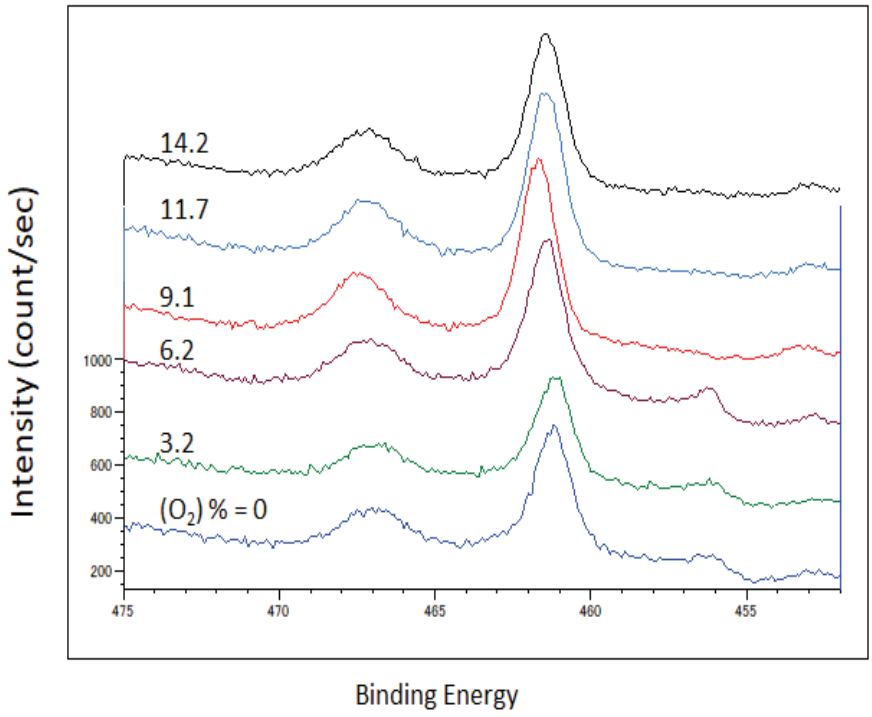

Fig. 3-9. XPS analysis results.

In order to confirm the hypothesis, XPS analysis was conducted. Fig. 3-9 shows the XPS analysis results. XPS studies were conducted for samples at the middle of glass tube at position Z3 (22.5 cm) to understand the chemical environment of titanium in the presence of different fraction of O_2. The characteristic peak of metal titanium for binding energy around 456 eV was observed under the conditions of f_{O2} at 0%, 3.2%, and 6.2%. This confirms the explanation for the above results in Figs. 3-7 and 3-8. Furthermore, a peak of non-stoichiometric oxide around 261 eV was observed for different conditions even for f_{O2} at 0%, which suggest that the film deposited at f_{O2} = 0% was oxidized. As the result of XPS shows that the upper surface of the film was oxidized even at f_{O2} = 0%, that can be attributed to oxidation happens when films were removed from chamber and exposed to atmosphere. On the other hand, in the absence of oxygen, the result for the resistivity shows that the inner part of the film was not oxidized at f_{O2} = 0% Considering these two results, only the surface of the film was oxidized at f_{O2} = 0%.

The increase in film resistivity will decrease the shifting velocity of plasma along the tube and that will affect the extended anode effect. Thus, this increase in the film resistivity affected the shifting velocity of main plasma position along the tube, as the shifting velocity decreased with increasing the electrical resistivity of the deposited film. Furthermore, the shifting velocity of main plasma position along the tube was influenced by decreasing of deposition rate by the decreasing electron density caused by the negative ion production. This will be discussed later.

Figure 3-10 shows film thickness as a function of axial position. This graph indicates the obvious difference in film thickness for $f_{O2} \leq 9.1$, which has smaller film thickness due to decreased plasma density by negative ion production and/or the

formation of TiO_2 film with higher electrical resistivity. Therefore, extended anode effect seems to work only for conductive films like Ti film in this experiment for $f_{O2} \leq 9.1\%$.

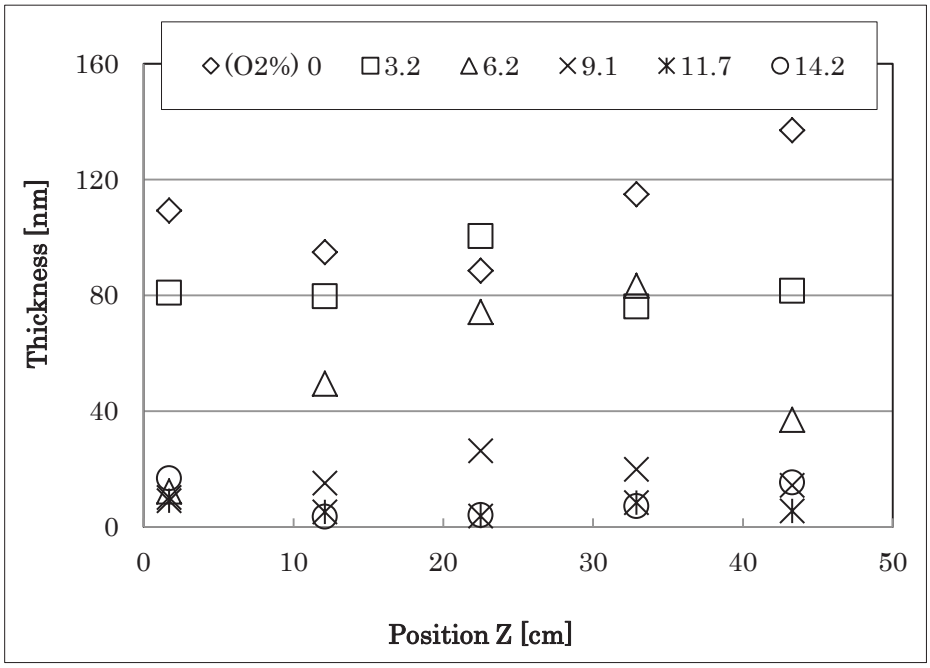

Fig. 3-10. Film thickness as a function of axial position.

Negative ions are produced during the sputtering time because of the presence of O_2, the reaction is shown by Equation 3-2.

$$O_2 + 2e^- \rightarrow O^{2-} \qquad (3\text{-}2)$$

During sputtering time, negative ions will be produced, and these negative ions and electrons will be attracted to the tube (anode). Since the target is cathode, electron density would be decreased and plasma generation might be ceased for long exposure time. Thus, the production of negative ions leads to a decrease in the electron density and to a decrease of the thickness of TiO_2 thin film. However, the use of pulsed power helps in reducing the effect of negative ions production by means of pulse off-time. As

refreshing time, pulse off-time is indispensable for sustaining the plasma generation and for relatively high density plasma. Because negative charges accumulate on the inner walls of glass tube (anode) during the on-time, electrons and negative ions repel each other during the off-time. The electrons move toward the inner conductor owing to the reverse field generated by the accumulated charge. The current pulse during the off-time will indicate the electron flow.

3.4 Brief summary

For uniform tube inner coating of non-conductive thin films, the extended anode effect in double-ended coaxial magnetron pulsed plasma was investigated. Coating has been performed for various thin films from metal to ceramic such as TiO_2 or TiN with different electrical conductivity. The deposited film profile and thickness were changed by the film electrical resistivity. Therefore, it can be concluded that the extended anode effect is strongly influenced by the electrical resistance of coated thin film on the inner surface of insulator tube. Moreover, the shifting velocity of the main position of plasma was affected by the production of negative ions in case of O_2. The effect of the production of negative ions can be seen in the difference of shifting velocity of the main position of plasma along the tube between the thickness profile of TiO_2 film and TiN film. Since shifting velocity was smaller for O_2 comparing to N_2, TiN film was supposed to reach anodic state faster than TiO_2 film. From the above, other methods for uniform coating of non-conductive thin film on the whole inner surface of insulator tubes should be developed.

References

[C1] H. Ohta, K. Inoue, Y. Yamada, S. Yoshida, H. Fujiyama, and S. Ishikura, Microgravity flow boiling in a transparent tube, Proc. of the 4th ASME-JSME Thermal Engineering Joint Conf., Lahaina, Hawaii, United States (1995), p.547.

[C2] J. A. Sheward, The coating of internal surfaces by PVD techniques, Surf. Coat. Technol. **54/55**, 297 (1992).

[C3] R. Hytry, W. Moller, R. Wilhelm, Running discharge for PECVD inner coating of metal tubes, Surf. Coat. Technol. **74-75**, 43 (1995).

[C4] T. Kraus, R. Kern, B. Stritzker, W. Ensinger, An advanced apparatus for ion beam assisted sputter coating of the inner walls of tubes, Nucl. Instrum. Methods Phys. Res. B, **148**, 912 (1999).

[C5] W. Ensinger, Corrosion and wear protection of tube inner walls by ion beam sputter coating, Surf. Coat. Technol. **86/87**, 438 (1996).

[C6] A. Schumacher, G. Frech, G. K. Wolf, A novel method for inside-coating of tubes and hollow cylinders by ion beam sputtering 1, Surf. Coat. Technol. **89**, 258 (1997).

[C7] H. Fujiyama, Y. Tokitu, Y. Uchikawa, K. Kuwahara, K. Miyake, K. Kuwahara and A. Doi, Ceramics inner coating of narrow tubes by a coaxial magnetron pulsed plasma, Surf. Coat. Technol. **98**, 1467 (1998).

[C8] Y. Uchikawa, S. Sugimoto, K. Kuwahara, H. Fujiyama and H. Kuwahara, Titanium coating of the inner of a 1 m long narrow tube by double-ended anode coaxial magnetron-pulsed plasmas, Surf. Coat. Technol. **112**, 185 (1999).

[C9] D. Xue, Y. Chen, G. Ling, K. Liu , C. Chen , G. Zhang, Preparation of aluminide coatings on the inner surface of tubes by heat treatment of Al coatings electrodeposited from an ionic liquid, Fusion Engineering and Design **101**, 128 (2015).

[C10] M. Ueda, AR. da Silva, EJ. Pillaca, SF. Mariano, Rde M. Oliveira, JO. Rossi, CM. Lepienski, L. Pichon, New method of plasma immersion ion implantation and also deposition of industrial components using tubular fixture and plasma generated inside the tube by high voltage pulses, Rev. Sci. Instrum. **87**, 013902 (2016).

[C11] S. Sugimoto, Y. Uchikawa, K. Kuwahara, H. Fujiyama and H. Kuwahara, Extended anode effect in coaxial magnetron pulsed plasmas for coating the inside surface of narrow tubes, Jpn. J. Appl. Phys. **38**, 4342 (1999).

Chapter 4

Tube inner coating of non-conductive films by pulsed reactive coaxial magnetron plasma with outer anode

4.1 Introduction

As mentioned in the previous chapter, double ended coaxial magnetron pulsed plasma (DCMPP) method was proposed for coating of the inner walls of narrow tubes with the aid of extended anode effect [D1]. The extended anode effect is useful for coating of conductive film inside insulator tube, because the deposited film plays the role of anodes [D1]. However, the extended anode effect cannot be used for insulator tube coating of non-conductive or high resistivity films, because electrons charge up on the tube inner walls and that prevents plasma from spreading along the tube as reported in our previous article [D2]. Therefore, new methods for uniform coating of non-conductive or high resistivity films on the inner walls of insulator tubes are required. Here, the author improved DCMPP method and developed a new method introducing a grounded aluminum foil which covered the outside of the glass tube to work as an auxiliary outer anode in the DCMPP method.

4.2 Experimental method

The experimental apparatus for tube inner coating by double-ended coaxial magnetron pulsed plasmas (DCMPP) is shown in Fig. 4-1.

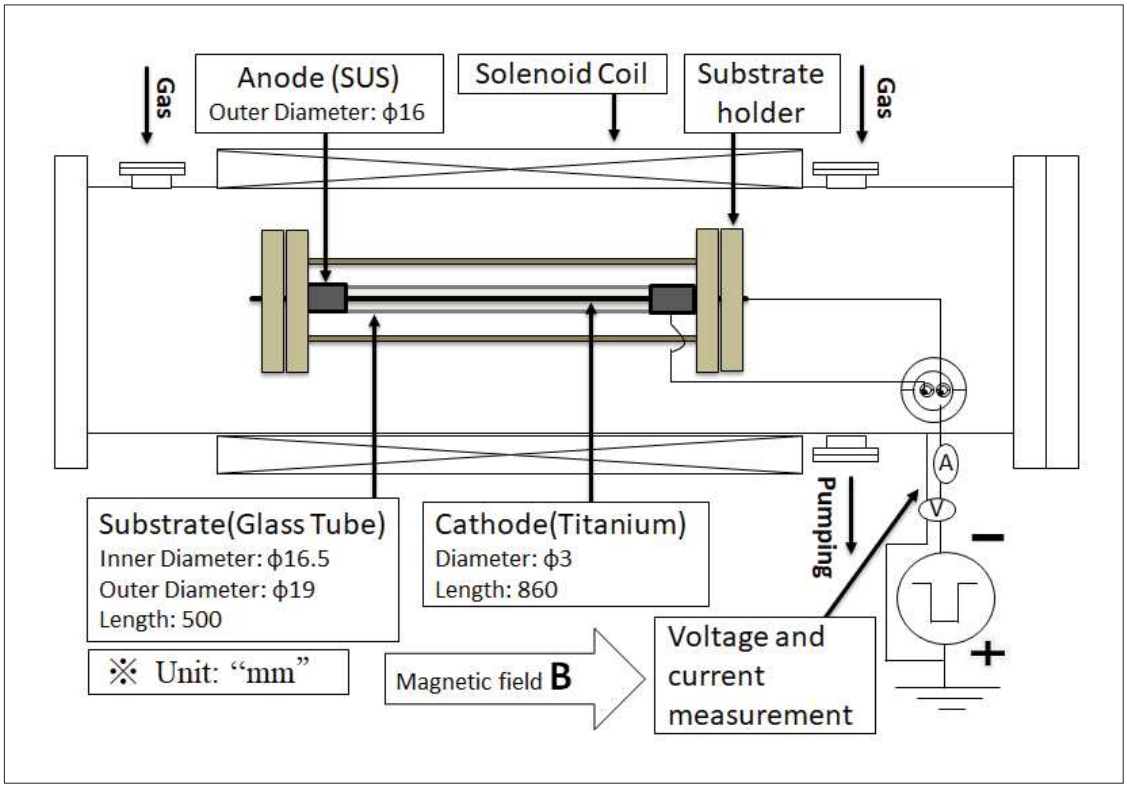

(a) Overall setup

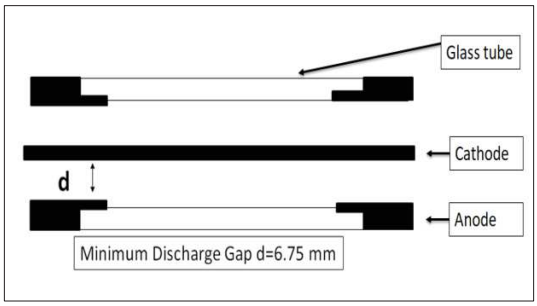

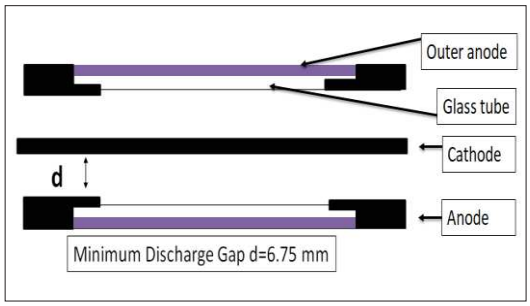

(b) Details of edge anode (c) Details of outer anode

Figs. 4-1. Experimental apparatus (a) overall setup, (b) details of edge anode, and (c) shows the details of outer anode. The white parts indicate the glass tube and the black parts at the edge of the glass tube are the ring anodes.

A long cylindrical vacuum chamber, 1300 mm in length and 320 mm in inner diameter, was used, and a water-cooled solenoidal coil was arranged coaxially around

the chamber to generate magnetic field as shown in Fig. 4-1(a). The anode consisted of stainless steel (SUS) ring electrodes positioned at both ends of the tube as shown in Fig. 4-1(b). The glass tube was 19 mm in outer diameter, 16.5 mm in inner diameter, and 500 mm in length. The part of the glass tube to be coated was only 435 mm in the middle of the tube, because the uncoated parts at both edges were covered with SUS ring anodes. The minimum discharge gap was 6.75 mm as shown in Fig. 4-1(b). The glass tube was completely wrapped with a grounded aluminum foil from the outside as shown in Fig. 4-1(c). This aluminum foil plays a role of an auxiliary outer anode which enhances the axial uniformity of the deposited film thickness as discussed later. A long fine cathode (a titanium rod of 3 mm in diameter) was positioned at the center of the glass tube.

The coating was performed by applying pulsed voltage between the anode and cathode under the following experimental conditions: Magnetic flux density at 833 G, gas pressure at 1 Pa, mass flow rate of Ar at 100, 90, 80, 70, 60 or 50 SCCM. Oxygen gas was used to obtain non-conductive films, so the fractions of O_2 was varied under constant fractions of Ar. Axial strong magnetic field (833 G) was applied in order to make the breakdown easier in a narrow tube under low-pressure conditions. The magnetron effect confines the electrons near the target, and increases the probability of collisions between the electrons, ions, and atoms [D3]. Consequently, pulsed discharge is generated between the long fine cathode and the grounded anode. In this study, we applied the frequency of 100 kHz. The applied power, the duty cycle and the sputtering time were set at 300 W, 55% and 2 min (15 sec×8), respectively. We also performed the coating without the outer anode for clarifying the effect of the outer anode.

The methods of measurement of the thickness and the resistivity of the coated film

have been already explained in the previous chapter.

4.3 Results and discussion

4.3.1 Coating of non-conductive films by DCMPP

Figure 4-2 shows the relationship between the thickness of the coated film and the fractions of O_2 without auxiliary outer anode. This graph shows that the coated film thickness decreases with increase of the fractions of O_2 in the gas mixture.

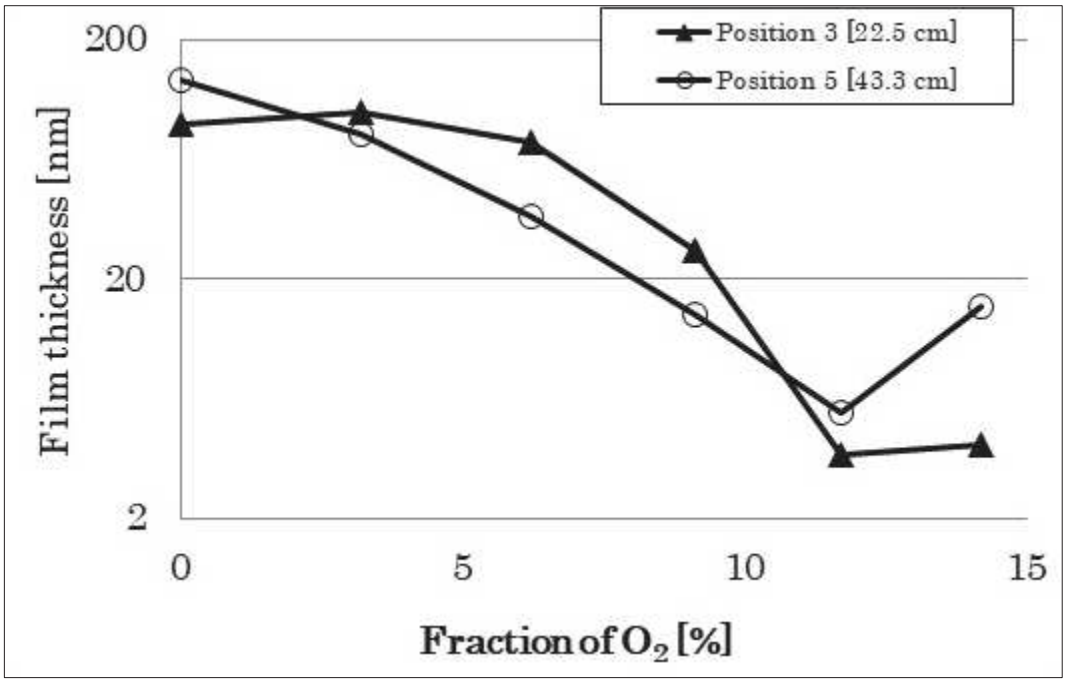

Fig. 4-2. Relation between the film thickness and the fractions of O_2 [%] in the case without Al auxiliary outer anode at the axial positions of 22.5 and 43.3cm from the edge of glass tube.

Figure 4-3 shows the relationship between the resistivity of the coated film and the fractions of O_2. This graph indicates that the resistivity increased with the fractions of O_2, and the property of the deposited film changed from metallic Ti to oxide TiO_2 at 9.1% of the fractions of O_2. Under that condition, the film with relatively high resistivity (more than 10^{-3} Ωm) was produced. The increase of fractions of O_2 leads to the production of negative ions. When the coated film is conductive, the deposited film plays a role of an anode to spread plasma along the tube and the ions are neutralized through the conductive film. On the other hand, when the coated film is non-conductive, the ions deposit on the insulator glass and on the non-conductive film. Thus, the charge accumulation of the surface of the film depends on the resistivity of the film. In the case of non-conductive or high resistive film, the major parts of the ions are deposited around the ring anodes and the electric field in the tube is affected by the deposited charges. Consequently, the plasma density was supposed to be reduced and the film became thinner compared to the cases of the fractions of O_2 less than 9.1%, as shown in Fig. 4-3.

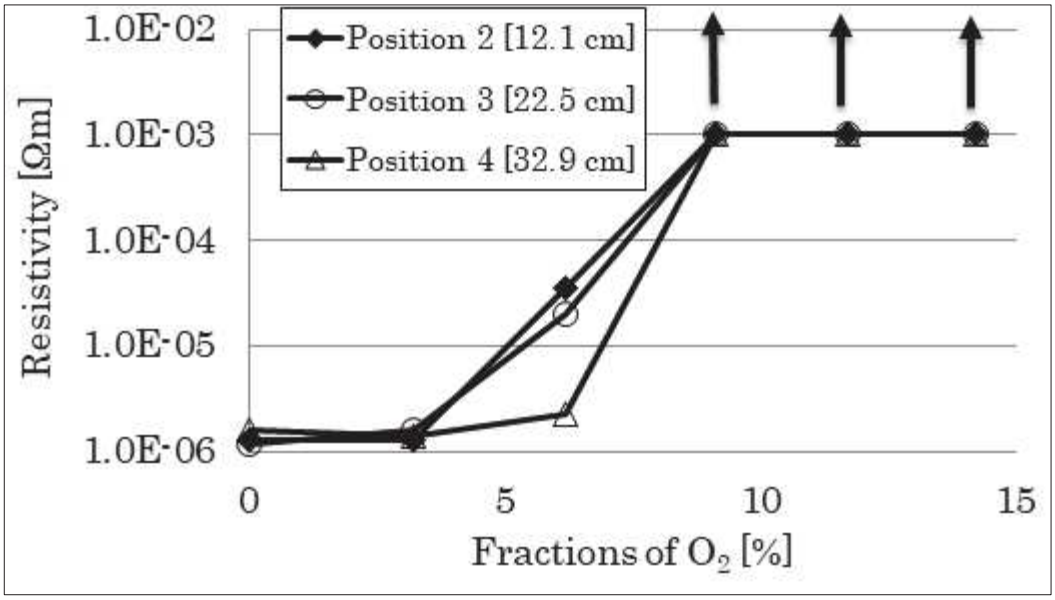

Fig. 4-3. Relation between the resistivity and the fractions of O_2 [%] in the case without Al outer anode at different positions.

Figure 4-4 shows the distribution of the thickness of the coated film as a parameter of the fractions of O_2 without outer anode. Three types of the distributions are recognized: they are almost flat distribution at low fractions of O_2, a convex shape distribution at middle fractions of O_2, and a concave shape distribution at high fractions of O_2. The thickness of the deposited film decreased with the fractions of O_2. This phenomenon can be attributed to the plasma density distribution affected by the change of the electric field distribution along the tube due to the change of the coated film resistivity.

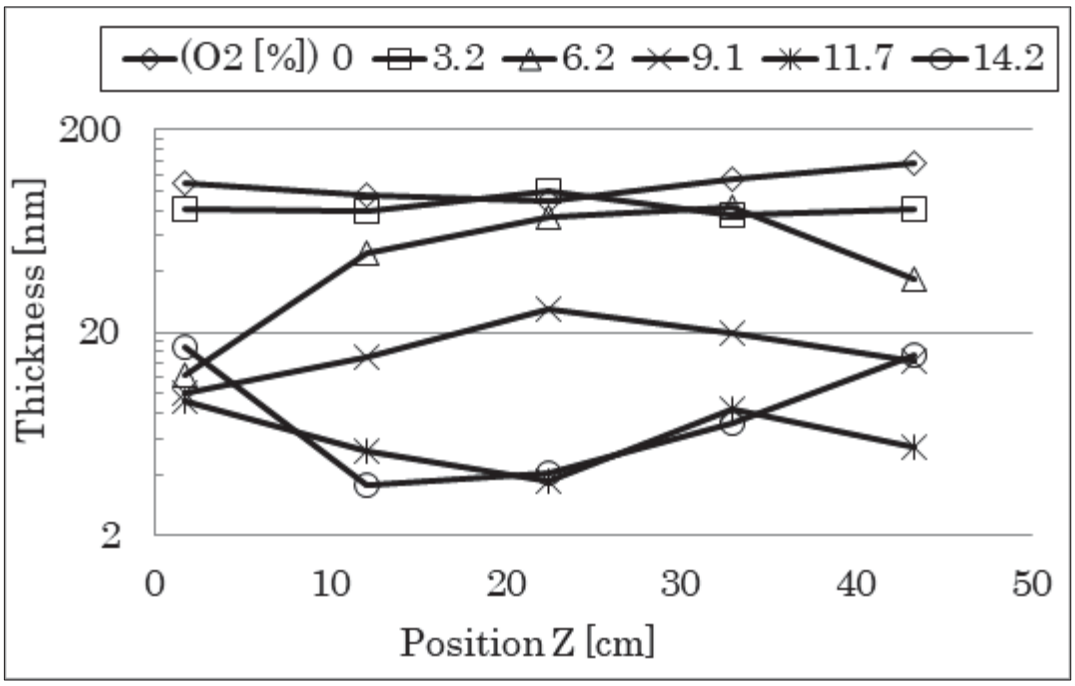

Fig. 4-4. Distribution of the film thickness along the axial position at different fractions of O_2 [%] in the case without Al outer anode.

4.3.2 Coating of non-conductive films by DCMPP with outer anode

Figure 4-5 shows the thickness distributions as a parameter of the fractions of O_2 with outer anode. The results reinforce the findings in Fig. 4-4. Higher resistivity of the coated film leads to production of thinner film. The criterion of the fractions of O_2 for coating of non-conductive film was around 9.1%. The films in Fig. 4-5 have better thickness uniformity which can be attributed to the presence of outer anode.

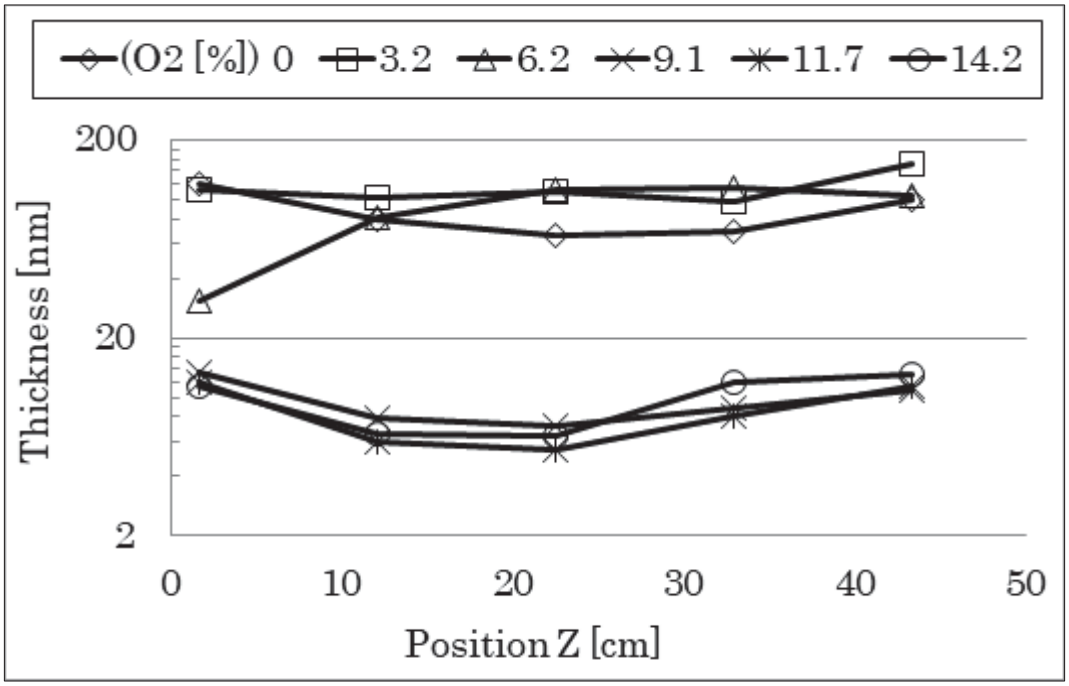

Fig. 4-5. Distributions of the film thickness along the axial position at different fractions of O_2 [%] in the case with Al outer anode.

Figure 4-6 shows the relationship between the resistivity of the coated film and the fraction of O_2 in the case with Al outer anode. This graph indicates that the resistivity increased with the fraction of O_2, and the property of the deposited film changed from metallic Ti to oxide TiO_2 at 9.1% of the fraction of O_2.

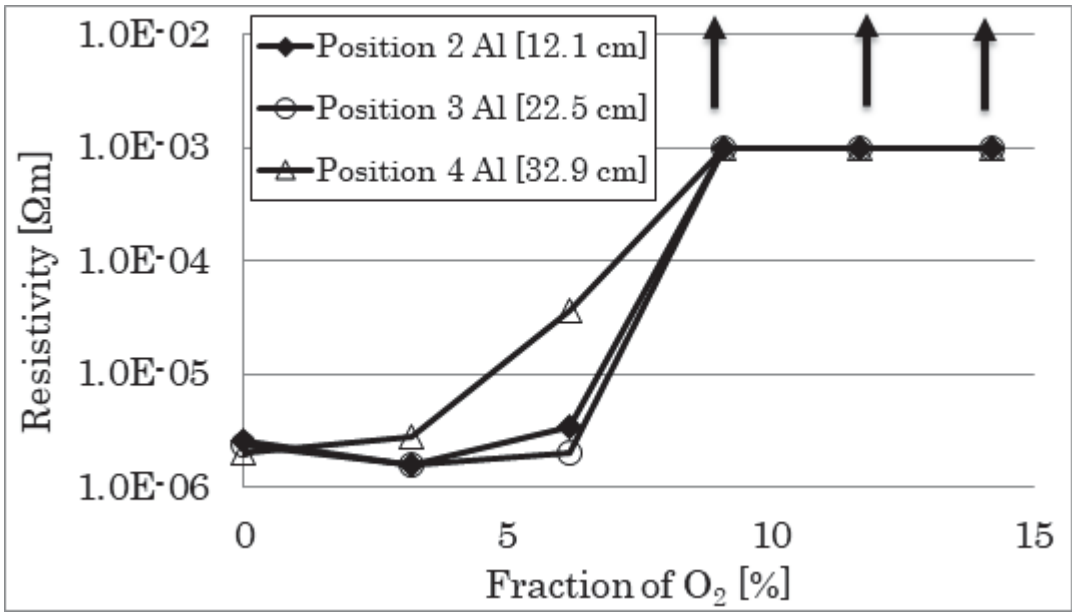

Fig. 4-6. Relation between the resistivity and the fraction of O_2 [%] in the case with Al outer anode at different positions.

Figure 4-7 shows the comparison of the uniformity of the film thickness between the cases with and without outer anode. The fraction of O_2 was 9.1 %. The electron density was supposed to decrease as the fractions of O_2 increased because the electrons attached to the O_2 molecules.

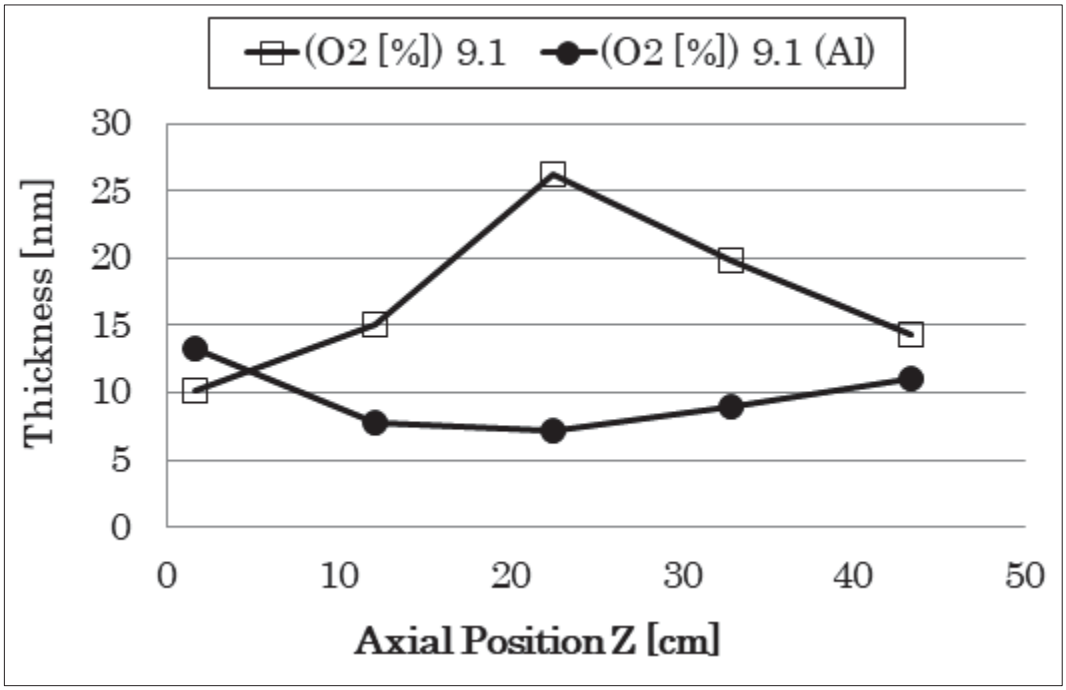

Fig. 4-7. Comparison of the deposited film thickness distribution along the axial position (Z) between the cases with and without Al outer anode (the fractions of O_2 is 9.1%).

Figure 4-8 shows the comparison of the uniformity of the film thickness between the cases with and without outer anode. The uniformity was evaluated by normalizing the film thickness by the average thickness. The error bars show the maximum and the minimum thickness normalized by the average thickness. Figure 4-8 (a) shows the case without outer anode and (b) shows the case with outer anode. The film was smooth in both cases at the fraction of O_2 lower than 3.2% compared with the high fraction. On the other hand, the uniformity was better for the case with outer anode compared with the case without outer anode when the fraction was higher than 9.1%. The uniformity became improved with the outer anode at high fraction of O_2. The electron density was supposed to decrease as the fraction of O_2 increased because the electrons attached to

the O_2 molecules. It can be attributed to the production of negative ions which were accumulated on the inner wall of the glass tube. In addition the electron energy decreases owing to the collisions with O_2 molecules. Consequently the plasma density and the deposition rate were reduced.

From the above, using an auxiliary outer anode improved the axial uniformity of the deposited film thickness, and the validity of the suggested method in this study was made clear.

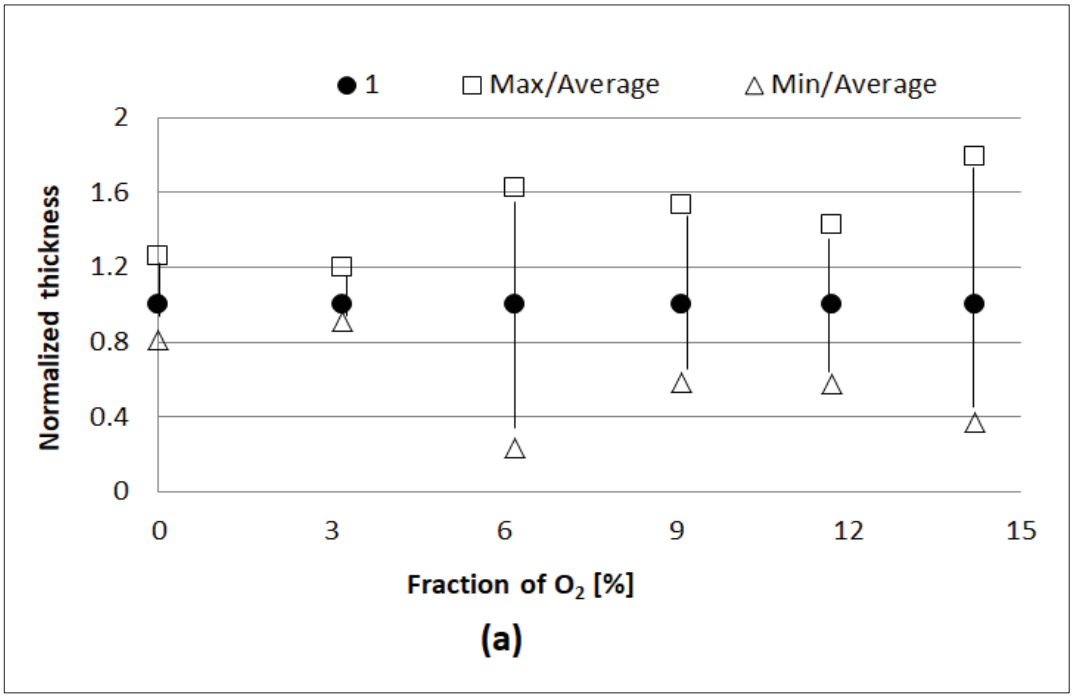

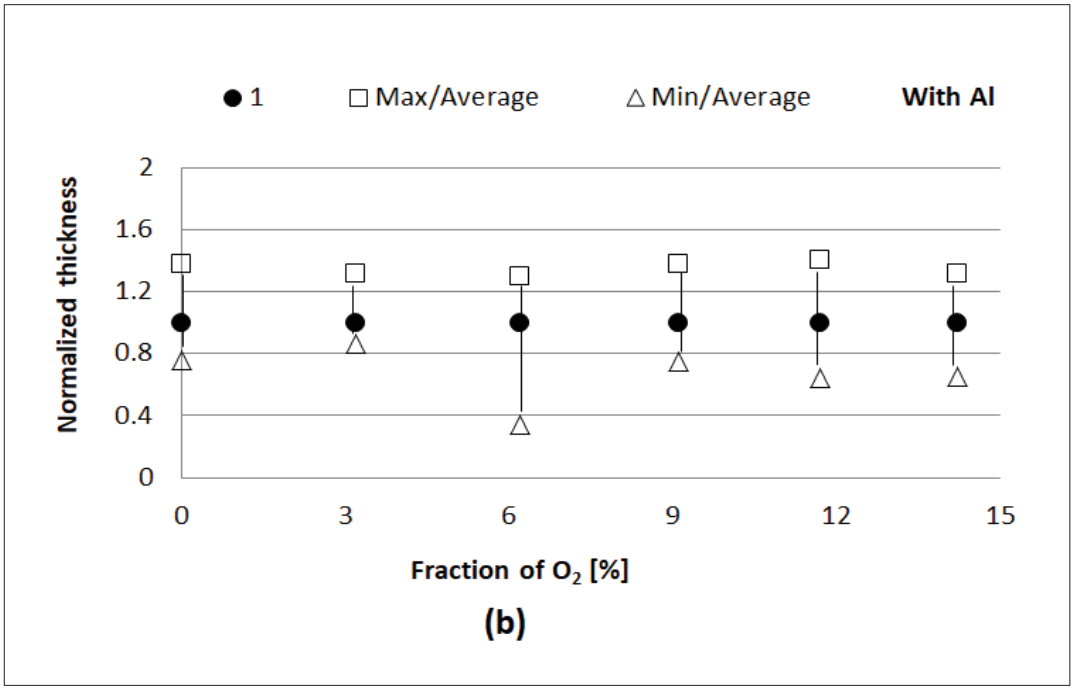

Fig. 4-8. Normalized thickness as a function of fraction of O_2 in the case (a) without Al outer anode, and (b) with Al outer anode.

4.3.3 Effect of outer anode on film coating by DCMPP

Figure 4-9 shows the characteristics of the DCMPP systems without using the auxiliary outer anode. Fig. 4-9(a) shows a schematic representation of the electric force lines around the glass tube. The plasma density can be estimated from the electric field distribution and is supposed to be higher in both edges of the glass tube than that in the middle. Fig. 4-9(b) shows the expected electric charges distribution on the glass tube coated by a non-conductive film. This figure illustrates the accumulation of negative charges on the inner walls of glass tube during the voltage pulse. Fig. 4-9(c) demonstrates an estimation of the film thickness distribution in the case of high resistance film. The deposited film supposed to be thicker at both edges of the glass tube owing to the high plasma density. However, the density of charge accumulation which is also higher compared with the middle of the tube decreases the electric field and consequently reduces the plasma density. In addition, the resputtering of the film can be considered around the anode. The resputtering phenomenon happens due to the bombardment of negative ions on surface of the deposited film, and consequently reduces the film thickness. Since the electric field is stronger at both edges of the glass tube, the likelihood for negative ions to gain enough energy for resputtering is higher at both edges of the glass tube. These phenomena have a role to reduce the thickness, however, they are complicated and depends on the fraction of O_2. Then, the thickness distribution is supposed to become the dashed lines depending on the fraction of O_2 as shown in Fig. 4-9(c).

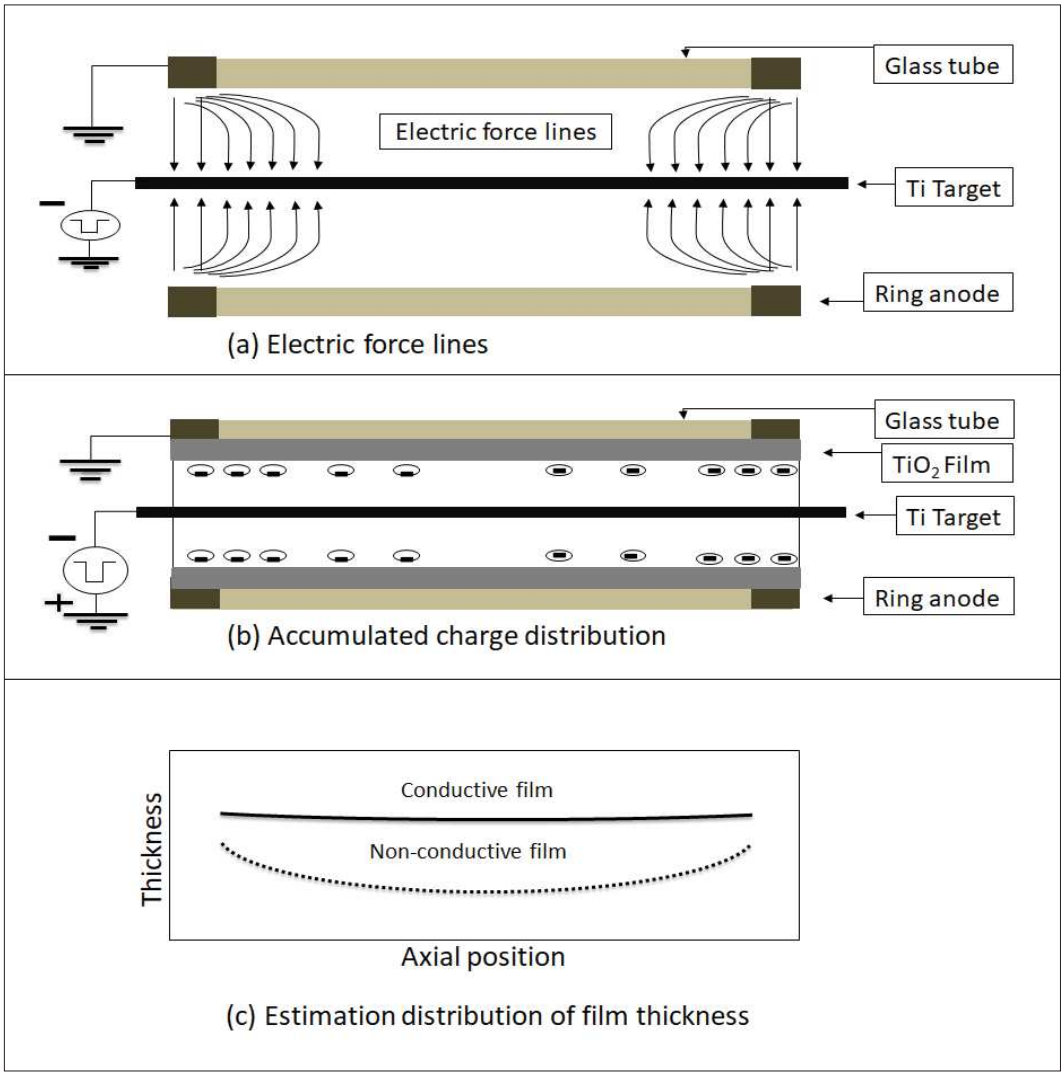

Figs. 4-9. Schematic representation of the electric force lines, electric charges distribution, and estimation of the film thickness distribution in the case without using Al outer anode. (a) A schematic representation of the electric force lines around the glass tube, (b) accumulated charge distribution around the glass tube, and (c) an estimation of the film thickness distribution in the case of high resistance film.

Figure 4-10 shows the characteristics of the DCMPP systems with the auxiliary outer anode. Fig. 4-10(a) shows a schematic representation of the electric force lines around the glass tube. The plasma density estimated from the electric field distribution

is supposed to be almost uniform. Fig. 4-10(b) shows the expected electric charges distribution around the glass tube coated by a non-conductive film. Then, the distribution of the electric charge is also supposed to be uniform. Although the deposited charge decreases the electric field, the effect is expected to be uniform. Fig. 4-10(c) shows an estimation of the film thickness distribution in the case of high resistance film deposited with outer anode. Since the uniform plasma density makes the film thickness uniform, the thickness distribution is supposed to become the solid line as shown in Fig. 4-10(c). The effect of the deposited charge which reduces the plasma density is also considered. When the effect is taken into account, the thickness distribution is supposed to becomes the dashed line as shown in Fig. 4-10(c).

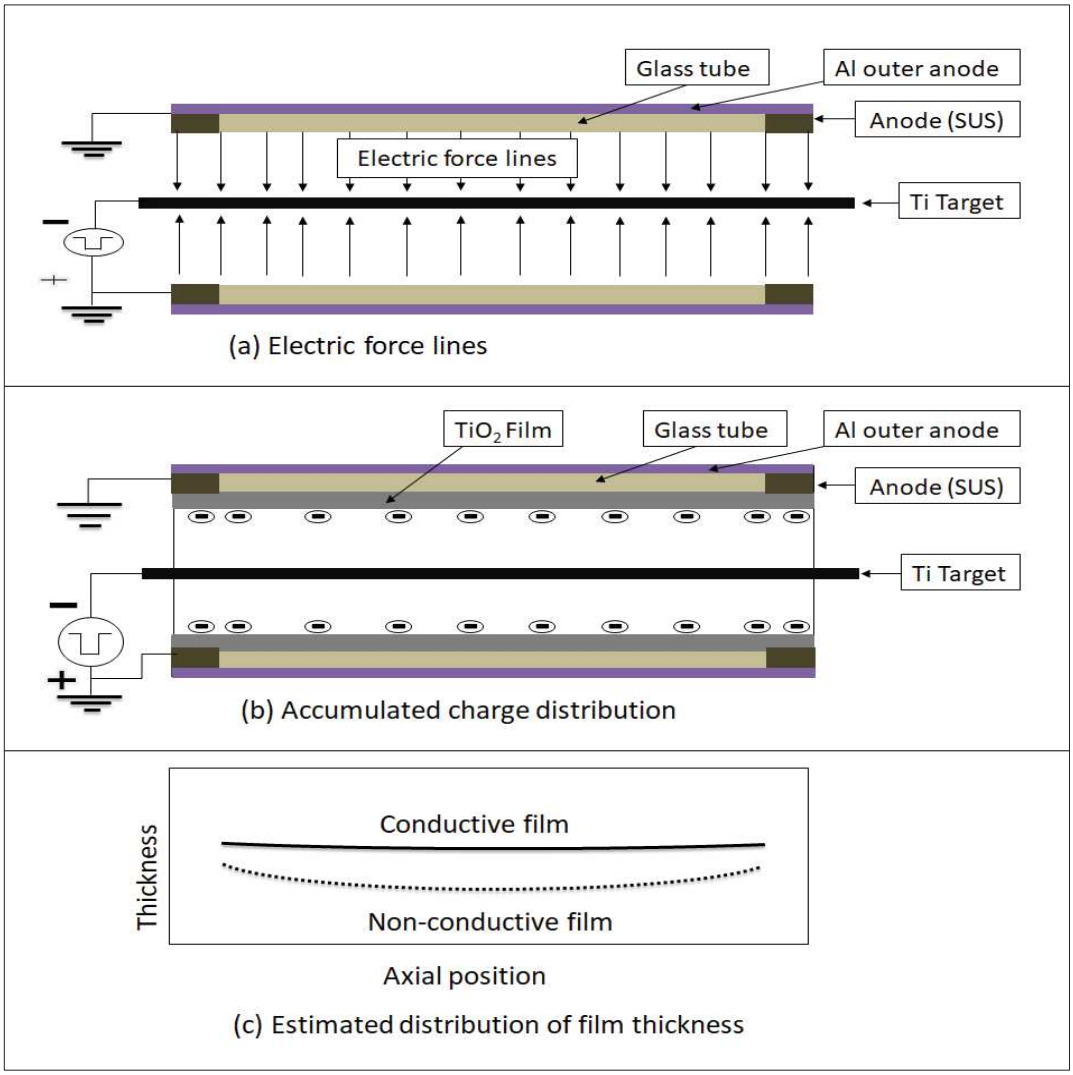

Figures 4-10. Schematic representation of the electric force lines, electric charges distribution, and estimation of the film thickness distribution in the case with using Al outer anode. (a) A schematic representation of the electric force lines around the glass tube, (b) accumulated charge distribution around the glass tube, and (c) an estimation of the film thickness distribution in the case of high resistance film.

As mentioned above, an outer auxiliary anode is expected to improve the thickness uniformity of a non-conductive coating on an inner surface of glass tube. Therefore, we synthesized an inner coating of a non-conductive film with a DCMPP system using an

outer auxiliary anode.

4.3.4 Further improvement in coating of non-conductive films

Figure 4-11 shows the voltage and the current characteristics as a function of the applied power frequency, where the power was set at 300 W. The current is an average current, and is supposed to mainly depend on the number of positive ions entering and sputtering the cathode. Therefore, higher frequency is better for sputtering.

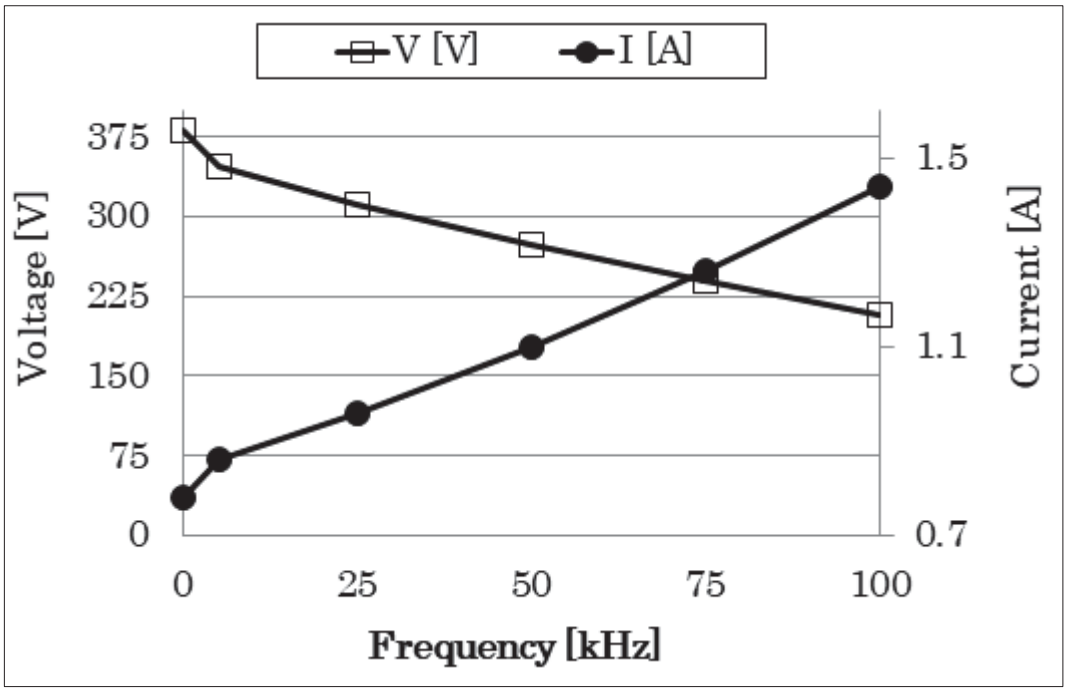

Fig. 4-11. Voltage and current characteristics as a function of frequency in the case without Al outer anode (the fractions of O_2 is 11.7%).

The off-time was important for the refreshment of discharges, because the accumulation of electrons and negative ions on the inner wall of glass tube consequently reduced plasma density. Fig. 4-12 shows examples of the voltage and current waveforms. The positive current pulse corresponds to the discharge current. On the other hand, the negative current pulse is supposed to be a current due to the space charge in the gap, which are driven by the inverse electric field caused by the charge accumulated on the film surface. The duration of the inverse current was 1-2 μs. From these waveforms, the off-time necessary for the refreshment is supposed to be 1-2 μs.

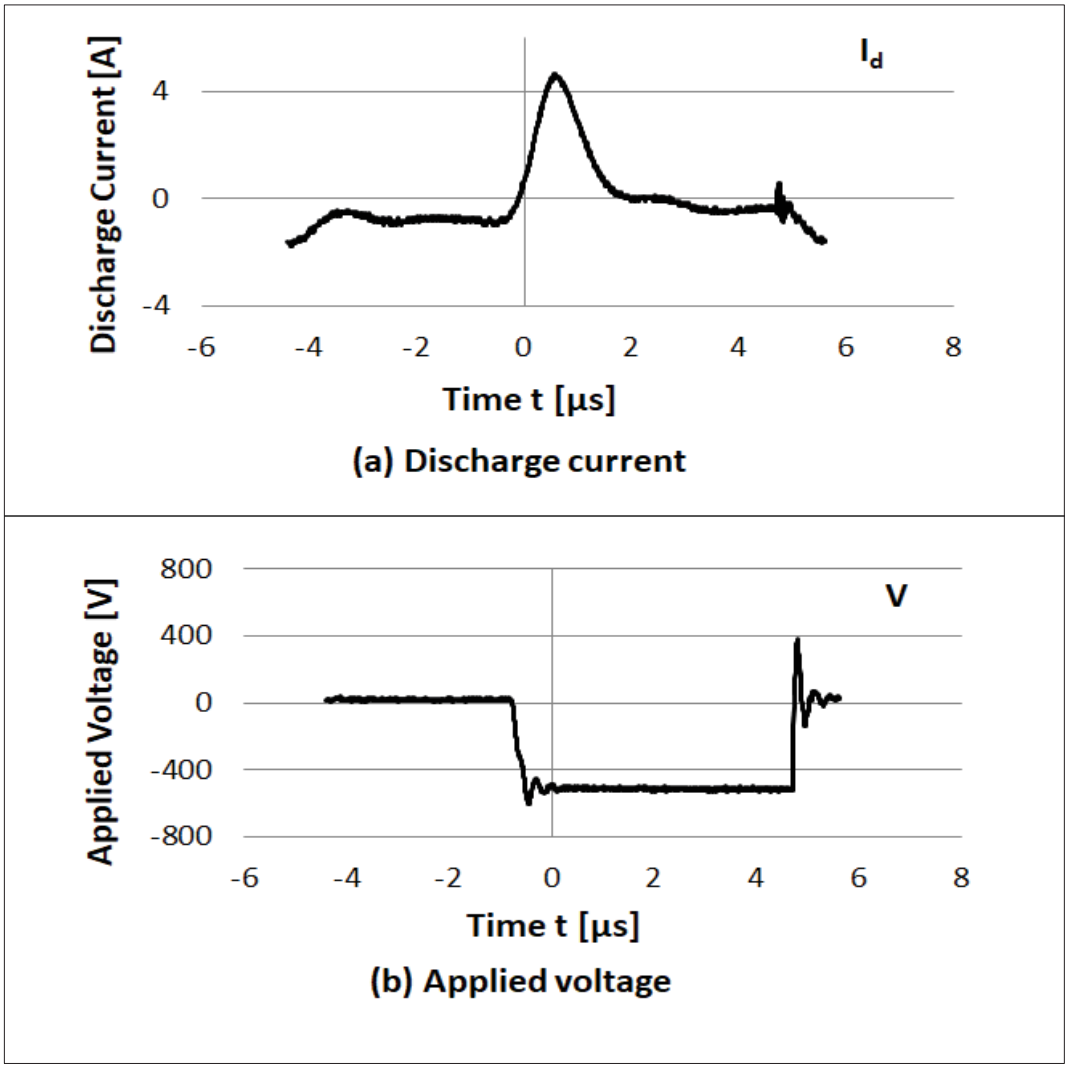

Fig. 4-12. Examples of the voltage and current waveforms in the case without Al outer anode (the fractions of O_2 is 6.2. %). (a) Discharge current, and (b) applied voltage.

4.4 Brief summary

The double-ended coaxial magnetron pulsed plasma (DCMPP) method with auxiliary outer anode was introduced in order to achieve a uniform coating of non-conductive thin films on the inner walls of insulator tubes. A comparison between films coated with and without an auxiliary outer anode was made for various fractions of O_2. As a result, it was clearly shown that using of auxiliary outer anode with DCMPP method improved the uniformity in the thickness of the deposited non-conductive TiO_2 film compared to DCMPP without an auxiliary outer anode. Moreover, it was revealed that the property of the deposited film changed from metallic Ti to TiO_2 at the fractions of O_2 around 9.1%. From the results, it was supposed that the auxiliary outer anode contributed to the uniformity of the distributions of deposited negative charge on the non-conductive film, electric field and the plasma density uniform.

References

[D1] S. Sugimoto, Y. Uchikawa, K. Kuwahara, H. Fujiyama, H. Kuwahara, Extended anode effect in coaxial magnetron pulsed plasmas for coating the inside surface of narrow tubes, Jpn. J. Appl. Phys. **38**, 4342 (1999).

[D2] M. T. I. Gasab, H. Sugawara, K. Sakata, H. Fujiyama, Extended anode effect for tube inner coating of non-conductive ceramics by pulsed coaxial magnetron plasma, Mater. Sci. Appl. **9**, 1 (2018).

[D3] P. J. Kelly, R. D. Arnell, Magnetron sputtering: a review of recent developments and applications, Vacuum **56**, 159 (2000).

Chapter 5

Conclusions

Coating with functional materials is attracting attention in various fields, because it can desirably change surface properties of materials. Plasma processing is widely used in coating, because a very wide variety of thin films can be deposited. However, it is very difficult to conduct inner coatings of narrow tubes. It is also difficult to conduct coating of non-conductive materials on non-conductive substrates. In this study, the author investigated on new methods to realize these challenging coatings in high performance. Consequently, the author has developed methods to conduct coating of non-conductive films on inner and outer walls of non-conductive tubes. The coated thin films were in acceptable performance. Major results are summarized as follows.

(1) The author developed a method to conduct coating of diamond-like-carbon (DLC) film on the outer wall of non-conductive flexible medical silicone tube (catheter) by a coaxial magnetron plasmas with multiple electrodes. The developed method is a hybrid technology of plasma vapor deposition (PVD) and chemical vapor deposition (CVD). The presence of DLC was confirmed by Raman scattering spectroscopy. Biocompatibility of DLC coating was verified by cell culturing. Raman spectrum also indicated the influence of plasma density on the size of carbon crystallites. In addition, friction test revealed that low friction coefficient DLC was obtained in low magnetic flux density.

(2) Validity of a double-ended coaxial magnetron pulsed plasma (DCMPP) method for coating on inner wall of non-conductive tube such as glass was investigated. As a result,

it is revealed that DCMPP method is effective for conductive film coating such as metal titanium (Ti), because of the extended anode effect. However, it is difficult to conduct uniform coating of non-conductive film such as titanium-oxide (TiO_2) or titanium-nitride (TiN).

(3) The results of coating on the inner wall of non-conductive tube showed that the thickness profile changed owing to the resistivity of the film. The thickness profile along the tube was also different between TiO_2 and TiN. From these results, the author supposed that the extended anode effect was affected by film resistivity and by the presence of negative ions caused by the presence of O_2.

(4) The author improved DCMPP method in order to conduct uniform coating of non-conductive thin film of titanium-oxide (TiO_2) on the inner wall of non-conductive tube such as glass. Finally, the author developed a hybrid method introducing an auxiliary outer anode to DCMPP method. It is revealed that the auxiliary outer anode improves uniformity of deposited film thickness.

Coating by plasma processing will progress further. I hope that the developed method will be widely applied and many coated products with high performance will be manufactured.

Acknowledgments

The author would like to thank Prof. T. Yamashita for his valuable guidance and supervision of this study, and for his scientific help. Also many thanks to Prof. H. Fukunaga for his continued guidance and for his supervision throughout the work as well as for the financial support to the author during several research internships. Also the author would like to Thank Associate Prof Y. Matsuda for his scientific help. Many thanks to Prof. S. Tanabe for his valuable comments, and for the scientific help. Also many thanks to Prof. M. Nakano for his valuable comments, and for the scientific help. Additionally many thanks to many fellow students for their contributions to this work.

Also many thanks to GEOMATEC Co Ltd. for several research internships and for the financial support for the author transportation between Nagasaki University and the internship venue, also many thanks to Mr. H. Sugawara of GEOMATEC Co Ltd. for the opportunity to conduct research internship at GEOMATEC Co Ltd. also many thanks to Mr. T. Sato, Mr. K. Sakata and Mr. M. Kato for the technical help. Also many thanks to Hitachi Metals, Ltd. for the internship.

Many thanks to Nagasaki University, Green system for the research grant, also many thanks to YEH KUO SHII Scholarship for the financial support, also many thanks to Nagasaki Kita rotary club for the financial support.

Special thanks and gratitude and firstly and foremost to Prof. emeritus H. Fujiyama, for his continued guidance and supervision all the way, and for his understanding and patience.